ANNUAL REVIEWS

Annual Review of Condensed Matter Physics

Swimming in Complex Fluids

Saverio E. Spagnolie[1] and Patrick T. Underhill[2]

[1]Department of Mathematics, and Department of Chemical and Biological Engineering, University of Wisconsin-Madison, Madison, Wisconsin, USA; email: spagnolie@math.wisc.edu

[2]Department of Chemical and Biological Engineering, Rensselaer Polytechnic Institute, Troy, New York, USA; email: underhill@rpi.edu

Annu. Rev. Condens. Matter Phys. 2023. 14:381–415

First published as a Review in Advance on December 16, 2022

The *Annual Review of Condensed Matter Physics* is online at conmatphys.annualreviews.org

https://doi.org/10.1146/annurev-conmatphys-040821-112149

Keywords

locomotion, soft matter, active matter, active suspensions, biological fluids

Abstract

We review the literature on swimming in complex fluids. A classification is proposed by comparing the length- and timescales of a swimmer with those of nearby obstacles, interpreted broadly, extending from rigid or soft confining boundaries to molecules that confer the bulk fluid with complex stresses. A third dimension in the classification is the concentration of swimmers, which incorporates fluids whose complexity arises purely by the collective motion of swimming organisms. For each of the eight system types that we identify, we provide a background and describe modern research findings. Although some types have seen a great deal of attention for decades, others remain uncharted waters still open and awaiting exploration.

1. INTRODUCTION

Biological fluids are messy. They can become more or less viscous by stirring them. They can store and release elastic energy across a wide range of relaxation timescales, or they can be soft in one direction and hard in another. Strange as they may be, these are the environments that microorganisms must often navigate in order to survive. A medium can even express astounding bulk features due to the emergent activity of the microorganisms themselves. The scientific literature on swimming in complex fluids is equally expansive—the phrase itself is used to describe physical systems that may seem hardly related.

The physics of swimming has captured the imagination for millennia (1), but advanced theories treating the locomotion of bodies through fluids would not appear until the dawn of mathematical fluid mechanics, and the confluence of physics and biology in the twentieth century. The study of microorganism locomotion at the micron scale, where viscous dissipation dominates inertia, has now been a tremendously active research area for the better part of a century (2–6).

The earliest works produced a great understanding of swimming in idealized (Newtonian) fluids. The fluids through which microorganisms swim, however, are often endowed with highly nonlinear, non-Newtonian features when viewed at a continuum scale, including shear-dependent viscosity, elasticity, and other features that blur the lines between fluids and solids. A broader understanding of the role of complex fluids in biological systems, including and beyond the physics of locomotion, is achieved with each passing year (7). The importance of these complex fluid phenomena on self-propulsion depends on the length- and timescales of the body motion when compared with those of the environment. Just as the Reynolds number[1] measures the relative importance of inertial and viscous effects, so the Carreau, Weissenberg, Bingham, and Ericksen numbers measure the importance of shear-thinning, viscoelasticity, viscoplasticity, and anisotropy, respectively (10).

Some fluids are even complex as a consequence of microorganism activity if treating the suspension of swimmers as part of the material. Active suspensions or active matter can exhibit orientational order and elastic response, shear-dependent viscosity, and negative viscosity (11–15). In addition to the microorganisms and suspending material, the presence of boundaries, whether internal to the fluid or confining it externally, can contribute to the emergence of the complex features noted above. For a broader look at the literature on confinement of active particles see the review by Bechinger et al. (16).

Given the many interpretations and dimensions of "swimming in complex fluids," a classification system might prove useful. Such a system may help identify the most important features of a physical system and unify seemingly disparate effects. The purpose of this review is twofold. First we aim to outline such a classification for swimming in complex fluids. To identify distinct types, we consider the relationship of the swimmer(s) to the constituents or obstacles that provide the fluid with complex features through their relative lengths and timescales, and we consider the concentration of swimmers. The second goal of this review is to provide a review of the literature for each of these types and to draw connections between them. Although our classification is not all-encompassing, we hope that it provides organizational clarity on the tremendously diverse field of physical phenomena and biological behavior in the context of swimming.

[1]The Reynolds number, $\mathrm{Re} = \rho UL/\mu$, with μ being the fluid's viscosity, and L and U being characteristic length and velocity scales of the swimming body, respectively, is orders of magnitude smaller than one for microorganism locomotion (8, 9).

2. A CLASSIFICATION OF SWIMMING IN COMPLEX FLUIDS

> It was the misfortune of the *Proteus* and her crew to be pioneers into a realm that was literally unknown; surely a fantastic voyage if ever there was one.
>
> —*Fantastic Voyage* by Isaac Asimov (Reference 17)

With the aim of organizing the complex fluid phenomena that either affect or are caused by swimming microorganisms, we focus on the relationship between an individual swimmer and its environment. The environment is characterized by the distribution and behavior of "obstacles," broadly interpreted. There may be only one large obstacle, representing a rigid or deformable boundary. Or the obstacles might be much smaller than the swimming body, like polymers or long-chain proteins, which relax into their preferred configurations over an intrinsic set of timescales. When there are sufficiently many such obstacles they confer the fluid with bulk features like viscoelasticity and shear-dependent viscosity. The obstacles might move with a background fluid, might themselves compose the background fluid, or they might be nearly fixed in space, for example, if the obstacle is large or if it is composed of a cross-linked network of fibers.

Figure 1 shows eight extremes of interest in our classification system, organized in a three-dimensional space. The vertical axis is the relaxation timescale of the obstacle(s) relative to a timescale associated with swimming motion, T_{obs}/T_{swim}, often called the Deborah number, De (18). Depending on the context and the physical processes that produce the timescales, this ratio might instead be referred to as a Weissenberg number, or possibly by other names, as is discussed below. The horizontal axis is the length scale of the obstacle(s) relative to a length associated with the swimming body, L_{obs}/L_{swim}, which we term the Benes number,[2] Bn. Finally the third axis is the volume fraction of swimmers, ϕ. The location of a system in this three-dimensional space influences the relative importance of different effects and the behaviors observed and, from a mathematical perspective, the modeling approximations that are most appropriate. The ratio of length scales and concentrations determines whether the swimmers or obstacles appear as an effective continuum. The ratio of frequencies or timescales determines the extent to which the suspending medium's relaxation properties affect the dynamics. The concentration of swimmers determines the importance of interactions among groups of swimmers or active particles.

The classification is not all-encompassing, and there are physical systems that could lie in multiple domains or sit outside of it altogether. For instance, an additional timescale (and classification axis) not considered here is associated with the rate of viscous dissipation and determines the relative importance of inertia. Nevertheless we press on to discuss some of the fundamental features of the proposed organization. We begin with Type I systems, which at the extreme includes a single swimmer in a Newtonian fluid.

2.1. Small De, Small Bn, Small ϕ: A Single Swimmer and Small Rigid Obstacles (Type I)

In Type I systems, a single swimmer navigates an environment containing small obstacles that are effectively rigid on the timescale of swimming. At the extreme separation of length scales, far to the left in **Figure 1**, the obstacles might even be the fluid constituents at the molecular scale. Taking 10 μm as a characteristic swimmer size and comparing with the size of a single water molecule,

[2] In the fictional *Fantastic Voyage* by Jerome Bixby and Otto Klement, novelized by Isaac Asimov, Dr. Jan Benes perfects a technology to manipulate an object's size (17). His body's various complex fluids go on to pose swimming and other challenges to the miniaturized crew injected into him to save his life.

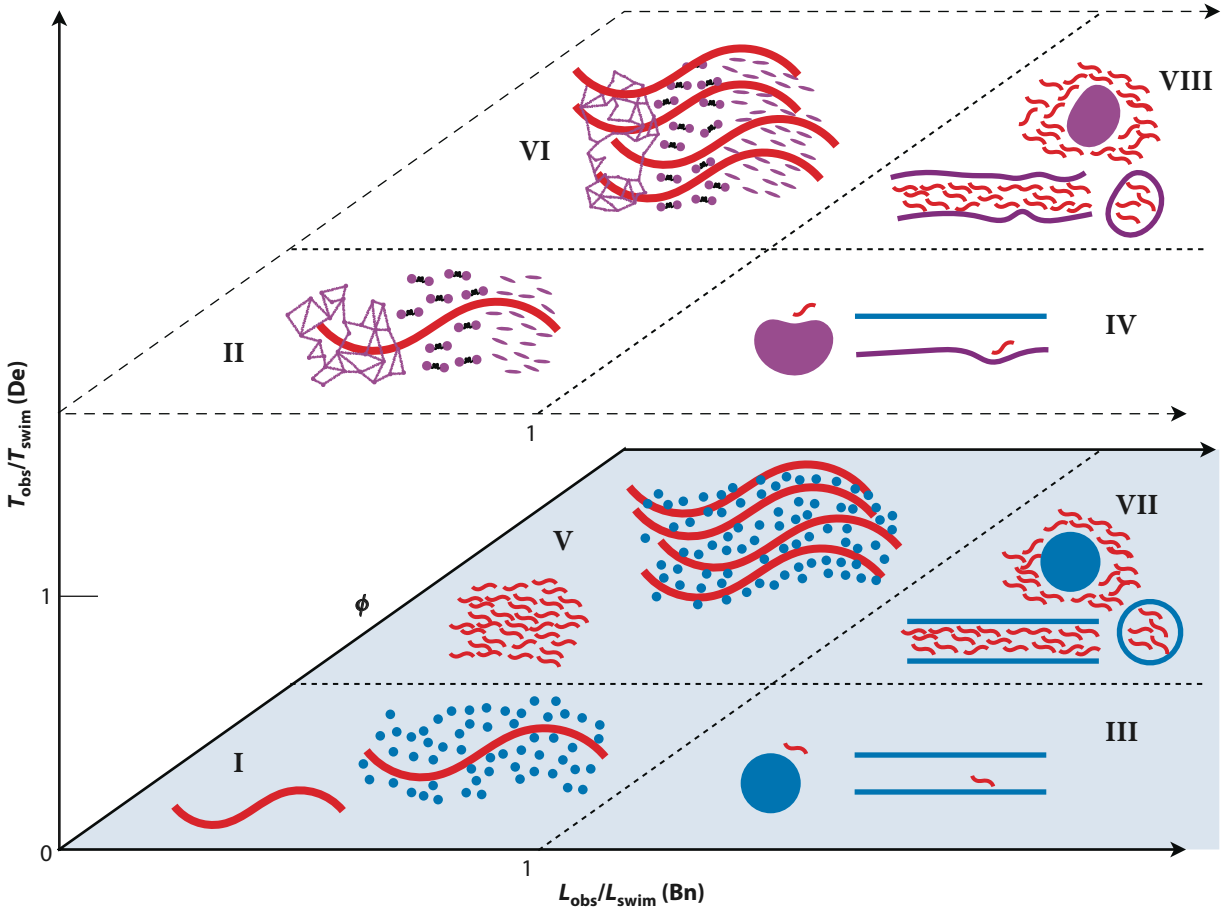

Figure 1

A classification of swimming in complex fluids. The axes are the lengths of the obstacle(s) relative to the swimmer, Bn = L_{obs}/L_{swim}, their relative timescales, De = T_{obs}/T_{swim}, and the volume fraction of swimmers, ϕ. Red objects are active (swimming), blue objects are rigid, and purple objects are deformable. (I/II) A single swimmer in a suspension of small rigid/deformable obstacles. (III/IV) A single swimmer near a large rigid/deformable obstacle. (V/VI) Many swimmers in a suspension of small rigid/deformable obstacles. (VII/VIII) Many swimmers near a large rigid/deformable obstacle. Abbreviations: Bn, Benes number; De, Deborah number.

we have Bn $\approx 10^{-3}$. Type I therefore includes swimming in classical Newtonian fluids, a familiar territory from which to depart on our journey.

The pioneering work on self-propulsion in viscous fluids appeared alongside improvements in microscope technology in the 1950s–1970s. Mathematical theories revealed many key features of swimming in Newtonian fluids at the microscale. They include instantaneously force- and torque-free dynamics, viscosity-independent swimming speeds for fixed gaits, kinematic reversibility (the "Scallop theorem"; 8), and widespread use of slender filament drag anisotropy (3, 5, 9, 19). Mathematical models from this era that remain mainstays across the field include Taylor's infinite swimming sheet (20), Lighthill and Blake's spherical envelope squirmer (21), and rotating helical model flagella (2).

Moving away from the origin and this Newtonian extremity, the rigid obstacles in question increase in size relative to the swimmer size. If still small compared to the swimmer but large

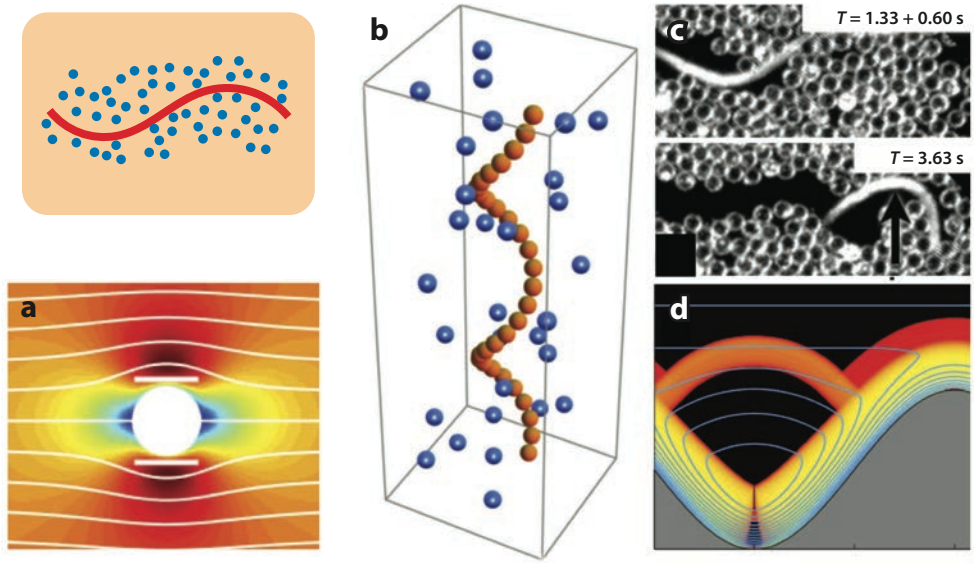

Figure 2

Type I systems: a single swimmer and small rigid obstacles. (*a*) Velocity magnitude of flow past a cylinder and streamlines in a model porous (Brinkman) medium—the additional anisotropy results in enhanced swimming speeds. Panel adapted with permission from Reference 22. (*b*) A helical filament swims faster in a heterogeneous environment of free obstacles. Panel adapted with permission from Reference 25. (*c*) *Caenorhabditis elegans* swims faster through a dense field of granular obstacles as it deforms the environment. Panel adapted with permission from Reference 26. (*d*) Density map of the shear rate (regions of zero shear-rate are *black*) near a swimming body in a viscoplastic medium at large Bingham number, showing local fluidization. Panel adapted with permission from Reference 27.

compared to the fluid's molecular constituents, they may still contribute features to the fluid that the swimmer experiences as a change in the bulk rheology. A porous medium, for example, which strongly affects the relationship between pressure and flow, can in turn have an effect on a relatively large swimming body. **Figure 2*a*** shows the velocity magnitude of a flow past a rigid cylinder in a model porous (Brinkman) fluid, which is associated with a particularly strong drag anisotropy. Such an environment was found to enhance undulatory and helical self-propulsion (22, 23). But decreased speeds were observed in the same medium for soft, deformable swimmers (22, 23) and for model tangential squirmers (24).

As the obstacles become larger, they have an even greater impact on swimming organisms. If they are fixed in space, their hydrodynamic reach is roughly independent of size—each appears as a Stokeslet singularity in the fluid flow, rather than as a higher-order stresslet disturbance field (28). Changes in swimming are even predicted at low obstacle volume fractions. Leshansky showed that the presence of stationary obstacles in the fluid increases the swimming speed and efficiency of a helical filament with a fixed rotation rate or even with fixed power input (**Figure 2*b***), essentially by pushing off of the surrounding obstacles (through the fluid; 25, 29). Experiments with *Caenorhabditis elegans* showed too an enhanced mobility in such environments owing to an increase in tangential/normal drag anisotropy (**Figure 2*c***; 26).

Greater obstacle volume fractions can result in additional complex features. The speed and efficiency of swimming in a viscoplastic fluid, which flows only beyond a critical stress, is characterized by the Bingham number, Bi, a characteristic ratio of the yield and viscous shear stresses.

Figure 2*d* shows the density of fluid shear rate, $\dot{\gamma}$, with regions of zero shear-rate also shown, near a swimming sheet at large Bingham number. Locomotion is critically dependent upon the fluidization of the environment local to the body surface and may involve the transport of plugged material regions (27, 30).

Type I problems also include systems with a yet broader view of swimming, like the locomotion of sandfish lizards and snakes through dry granular media (31, 32). So long as the relaxation time of the microstructure is small compared to the body's rate of motion, swimming through fluids with other unusual behavior may still appear as a Type I system. One such example is swimming in media with a fixed orientational order (e.g., a transversely isotropic fluid; 33–35). The local order often has a longer relaxation timescale, however, which takes us in the direction of Type II systems.

2.2. Large De, Small Bn, Small ϕ: A Single Swimmer in a Suspension of Small Deformable Obstacles (Type II)

> The antibodies lined up side by side, their spaghetti strand projections entangling.
>
> —*Fantastic Voyage* by Isaac Asimov (Reference 17)

In Type II systems the obstacles express their own relaxation features in a more significant way. They might be long-chain polymers, elastic networks or gels, or molecules that, though individually rigid, slowly relax together into order or to a disordered equilibrium state. Mammalian spermatozoa encounter several such complex fluids, including glycoprotein-based cervical mucus, mucosal epithelium inside the fallopian tubes, and actin-based viscoelastic gel outside the ovum (36, 37). The relaxation may also be diffusive in nature; a dilute suspension of rigid rods may become more aligned by a flow, only returning to an isotropic orientational distribution on a timescale set by the fluid viscosity and temperature.

2.2.1. Shear-dependent viscosity. Shear-dependent viscosity, shear-thinning in particular, appears often when a solvent is host to a suspension of small, immersed obstacles or highly deformable polymers. A suspension of elongated particles tends to align with a background shear flow, reducing the bulk viscous resistance. The Carreau number, $\mathrm{Cu} = \lambda\dot{\gamma}$, is a dimensionless rate of the timescale λ of the environment's relaxation process and the timescale associated with the local shear rate, $\dot{\gamma}^{-1}$ (38). Mucus, for instance, is significantly shear-thinning—with a relaxation time λ on the order of 1,000 s, its viscosity begins to drop at $\dot{\gamma} \approx 10^{-3}$ s^{-1}, then decreases by four orders of magnitude until $\dot{\gamma} \approx 10^{2}$ s^{-1} (39, 40). In a swimming system the relevant shear rate is often that generated by the motion of a swimming body, and the Carreau number is precisely the comparison of timescales $T_{\mathrm{obs}}/T_{\mathrm{swim}}$ in **Figure 1** (i.e., it could as well be called the Deborah number if the flow is oscillatory, or in a constantly sheared fluid the Weissenberg number, introduced below).

Depending on the fluid, swimming in such an environment could instead be classified as a Type I system, as the obstacles themselves need not have an intrinsic deformability or timescale to confer shear-dependent bulk properties. Even in the relatively simple environment composed of a solvent and a suspension of shear-aligning rigid rods, Brownian fluctuations introduce a relaxation timescale at the ensemble level. Fluid deformability might in this case be interpreted as the malleability of the distribution of obstacle orientations. A ratio of diffusive relaxation and flow timescales in this setting is generally called a Peclet number, Pe.

Experiments with the workhorse of undulatory locomotion, the nematode *C. elegans*, showed no substantial change in either the body kinematics or swimming speed in a shear-thinning xanthan gum polymeric solution (41; **Figure 3*a***). In a polystyrene colloidal suspension, however, the stroke

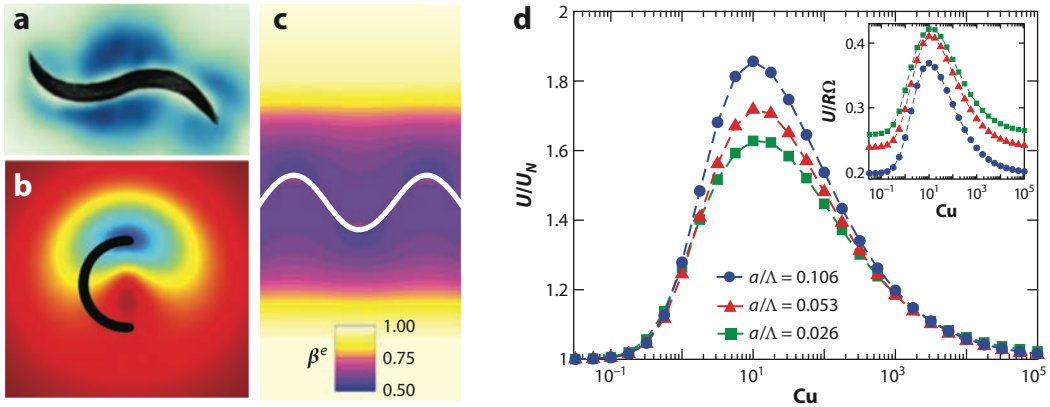

Figure 3

Type II systems: a single swimmer in a suspension of small deformable obstacles (shear-dependent viscosity). (*a*) Velocity magnitude near a swimming *Caenorhabditis elegans* nematode in a shear-thinning fluid. Panel adapted with permission from Reference 41. (*b*) Viscosity field due to the prescribed motion of a helical body in a shear-thinning fluid, resulting in swimming enhancement. Panel adapted with permission from Reference 42. (*c*) Similar viscosity stratification near a swimming sheet, also resulting in increased swimming speeds, with β^e being the viscosity relative to the zero-shear-rate viscosity. Panel adapted with permission from Reference 43. (*d*) A Goldilocks zone of Carreau numbers Cu for confinement-like swimming enhancement of helical bodies for a few filament aspect ratios. Panel adapted with permission from Reference 42.

form changed and swimming speeds increased by up to 12% while swimming efficiency continued to increase even once the swimming speed saturated (44). In this second effort, it was suggested that the effects were more apparent due to a larger viscosity contrast near the shear rates relevant to the swimming motion.

Helical swimmers in a shear-thinning fluid showed even greater speed increases of up to 50% in experiments (45) and beyond in simulations (**Figure 3*b***; 42). Similar results were found using model swimming sheets (43). **Figure 3*c*** shows the viscosity relative to the zero-shear-rate viscosity at large Carreau number owing to the undulatory motion of a swimming sheet with a prescribed motion, revealing a very large region of diminished viscosity. Rather than being the result of surface-localized viscosity reduction, it has been suggested that the speed enhancement is due to a confinement-like effect owing to viscosity stratification. The more viscous regions appear as confining walls, apparent in **Figure 3*b*,*c***, revealing a connection between Type II systems and Type III systems (43, 45, 46). The large amplitude body motions used in these numerical studies were also important—the effects of shear-dependent viscosity on the speeds of undulatory model swimmers enter only at fourth order in the dimensionless if small amplitude (39).

The swimming speed relative to the Newtonian swimming speed for helical swimming in a shear-thinning fluid is shown in **Figure 3*d*** as a function of the Carreau number. For both small and large Carreau numbers the environment has a nearly constant viscosity everywhere, and the fluid acts as an effective Newtonian fluid. Because the swimming speed of a body in a Newtonian fluid is independent of viscosity for fixed kinematics, the Newtonian swimming speed is recovered at these extremes. In the "Goldilocks zone" of Cu of order $1–10^3$, however, when the relaxation rate is comparable with the rate of body motion, the viscosity change has a more detailed spatial structure, and swimming enhancement is observed. Theoretical investigations using the model tangential squirmer, meanwhile, revealed a speed reduction in this range of Carreau numbers (47). The details of how the boundary conditions and the resulting viscosity stratification affect swimming are thus not always easy to guess.

2.2.2. Viscoelasticity. Shear-dependent viscosity is among the simplest non-Newtonian bulk fluid features to consider. Short-range interactions among constituent molecules, or intrinsic relaxation times, introduce more dynamic bulk properties. How do such bulk features affect swimming organisms? Unlike in Newtonian fluids, energy is temporarily bound into the fluid, which can either aid or resist self-propulsion. Extra fluid stresses can even change the shape of a swimming body or its motility organelles. Flagellar beating by spermatozoa becomes hyperactivated in viscoelastic fluids (**Figure 4*a***), improving their mobility (48). But viscoelastic environments can reduce swimming speeds as well, as observed in experiments using *C. elegans* (**Figure 4*b***; 49). See also the review by Sznitman & Arratia (61).

Such fluids are commonly characterized by the Weissenberg number, $\mathrm{Wi} = \lambda\dot{\gamma}$, yet again a product of a relaxation time, λ (here an elastic relaxation), and a shear rate, $\dot{\gamma}$. In swimming problems, the shear rate is often oscillatory owing to the periodic motion of motility organelles like flagella and cilia. Accordingly, the Deborah number $\mathrm{De} = \lambda\omega$ is more commonly used, where ω is the frequency of oscillation. The subtle distinction between the two depends on yet another length comparison. The magnitude of the shear rate in an oscillatory setting is $\dot{\gamma} = A\omega/L$, with A being the oscillation amplitude and L being the length scale of the oscillating body, thus $\mathrm{Wi}/\mathrm{De} = A/L$, which can be small or large in the same fluid. Many more details about Type II systems in particular can be found in recent reviews of swimming in viscoelastic fluids by Elfring & Lauga (62) and Li et al. (63), and of active colloids in complex fluids by Patteson et al. (64).

Viscoelastic model fluids like the Stokes/Oldroyd-B equations (38) have been used to show that speeds should decrease monotonically with the Deborah number for infinite swimming sheets (65, 66) and helical bodies (52, 67, 68) upon the steady propagation of small amplitude waves. For small amplitude perturbations to the fluid, frequency space provides a natural decomposition of viscous and elastic effects and explains why the same Deborah number dependence arises for both undulatory and helical motion (62, 69), even in confined systems (**Figure 4*c*,*d***; 51, 52). Mobility enhancement in a purely viscoelastic fluid thus requires large amplitude body motions, finite length, or asymmetric beating, which have been explored numerically with fixed kinematics (53), deformable bodies (54, 66, 70), and mixed wave speeds (71). **Figure 4*e*,*f*** shows the added polymeric stress near the tips of finite swimming sheets for fixed kinematics and for a deformable swimmer. These additional stresses can either aid or restrict propulsion depending on the nature of the stroke (53, 54). A spatially increasing wave amplitude introduces a flapping-like motion that would not generate a net thrust in a Newtonian fluid, owing to kinematic reversibility, but does in a viscoelastic fluid, leading to swimming enhancement (72). Near walls, the fluid pinned between the swimmer and a surface can experience large local strains and stresses that in turn can have an outsized effect (66, 73). Similarly, such large strains near the body may be created by swirling flows, either by the body or by rotating flagella; the hoop stresses so generated can also provide a boost to swimming speeds (74, 75).

Pathogen mobility in complex fluids is another area of interest for unsubtle reasons. Helical *Leptospira* and *Borrelia burgdorferi* cells, the root cause of Weil's and Lyme diseases, respectively, swim faster in viscoelastic environments (76, 77). Experiments using a Boger fluid (55) and numerical solution of the Stokes/Oldroyd-B equations (56) recovered such enhancements at large helical amplitudes (**Figure 4*g***). **Figure 4*b*** shows the swimming speed relative to the Newtonian swimming speed for bodies of different helical amplitudes across a range of Deborah numbers, with values over one achieved only beyond a critical large amplitude for both helical waves and rigid body rotation (56).

But relating experiments to simulations and theory can be complicated by the fact that shear-thinning and viscoelasticity often occur together in real fluids and can depend on distinct features acting simultaneously on multiple scales (46, 57). **Figure 4*i*** shows the viscosity of a polymeric

fluid as a function of polymer concentration using a rheometer, microrheology with a 980 nm bead, and microrheology using a small bead closer to the size of a flagellar cross-section (40 nm) showing no appreciable dependence on polymer concentration. On the scale of the flagellum, then, the resistance is merely due to the solvent viscosity, which was proposed as being due to

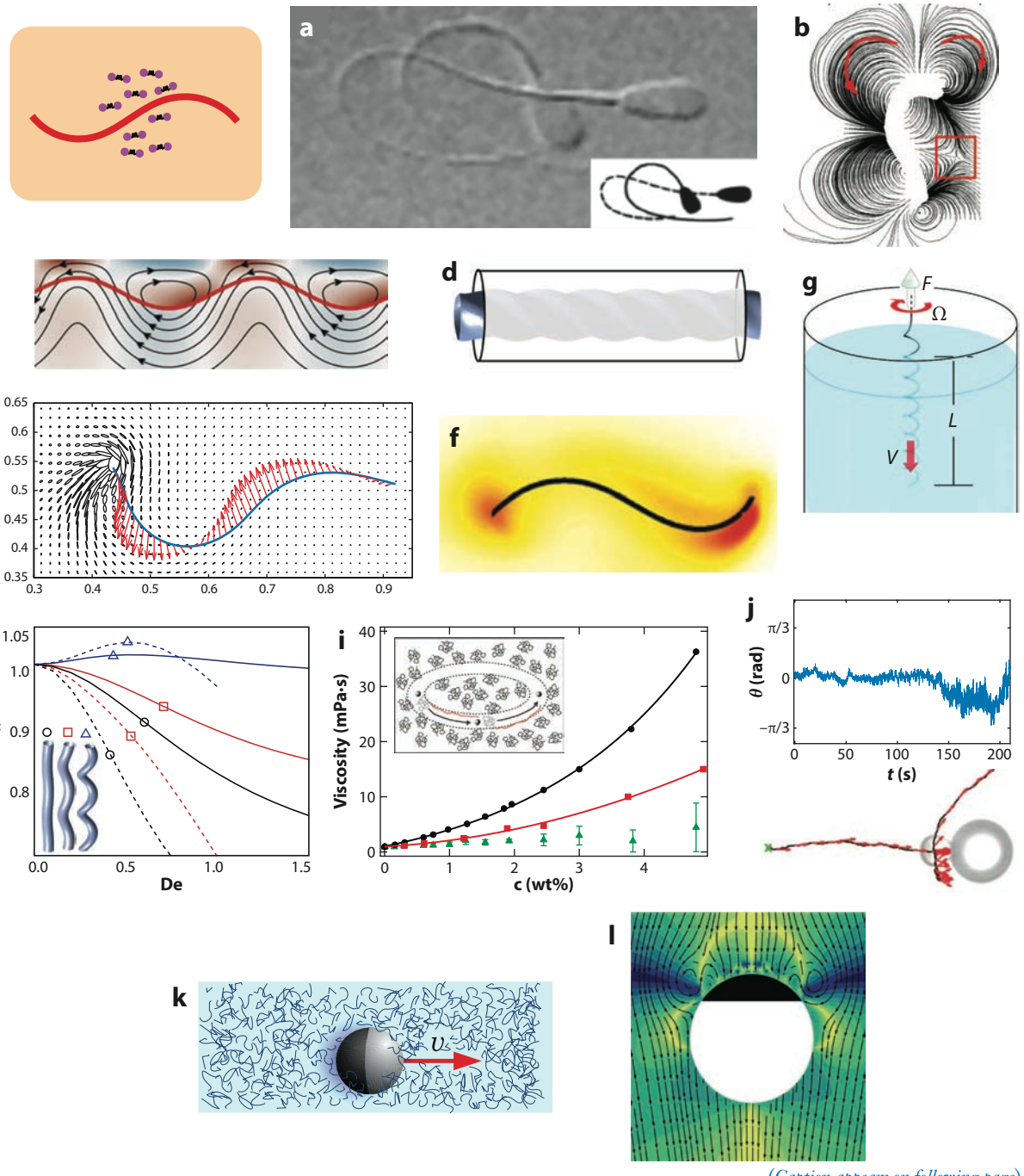

(*Caption appears on following page*)

Figure 4 (*Figure appears on preceding page*)

Type II systems: viscoelastic fluids. (*a*) Spermatozoa become hyperactivated and swim faster. Panel adapted with permission from Reference 50. (*b*) The motion of *Caenorhabditis elegans* creates stagnation points in the flow (e.g., in the *boxed region*) and slows swimming. Panel adapted with permission from Reference 49. (*c*) Streamlines generated by a swimming sheet near a boundary in a viscoelastic fluid. Panel adapted with permission from Reference 51. (*d*) Swimming and pumping are modified through the mode-dependent complex viscosity in a confined domain. Panel adapted with permission from Reference 52. (*e*,*f*) Focusing of polymeric stress near the tips of a swimming sheet (*e*) with a fixed gait (panel adapted with permission from Reference 53) and (*f*) with a stress-dependent gait (panel adapted with permission from Reference 54). (*g*) Schematic of an experiment showing enhanced propulsion of helical filaments in viscoelastic fluids. Panel adapted from Reference 55. (*h*) Scaled swimming speed across Deborah (De) numbers for three different helical amplitudes, by helical waves (*solid lines*) and rigid rotation (*dashed lines*) from simulations. Panel adapted with permission from Reference 56. (*i*) Viscosity of a polymeric fluid versus polymer concentration using a rheometer (*circles*), microrheology with a large bead (*squares*) and a flagellum-diameter-sized bead (*triangles*), suggesting strong shear-thinning at the finest scale (*inset*). Panel adapted with permission from Reference 57. (*j*,*k*,*l*) Tangential squirmers in viscoelastic fluids (*j*) with geometric confinement [panel adapted with permission from Reference 58 (CC BY 3.0)], (*k*) showing increased rotational diffusivity (panel adapted with permission from Reference 59), and (*l*) driven by autophoresis (panel adapted with permission from Reference 60).

severe shear-thinning in the region near the flagellum (57, 78). The fixed geometry of model tangential squirmers offers a simplified setting, useful for probing the roles of stroke asymmetry and geometric confinement (**Figure 4*j***; 58, 73), large changes in rotational diffusivity under external forcing (**Figure 4*k***; 59), and the coupling of autophoretic motion to the complex generated flow (**Figure 4*l***; 60). Methods and devices for using swimmers as rheometers continue to be developed, with a particular focus on future medical applications (79–81). We refer the reader to the particularly germane review by Venugopalan et al. (82).

2.2.3. Networks and gels. Rather than moving freely, the obstacles may instead be connected to each other. In this case, the relevant relaxation timescale(s) may be that of a porous or cross-linked network of fibers or a gel. **Figure 5*a*** shows a spermatozoan swimming through the elongated glycoproteic meshwork in cervical mucus, showing that the obstacle size is much closer to the swimmer size than is often appreciated. Using the pore size as an obstacle length scale, for microorganisms swimming through mucus the Benes number Bn can be in the range of 0.1–2 (83). Similar to the example of shear-thinning by a moving flagellum suggested by **Figure 4*i***, continuum theories using two-phase fluid models suggest that the nature of the network (and so the boundary conditions) on the swimming body are of critical importance for both swimming speed and efficiency (84, 85). Enhanced motion has been found for undulatory swimmers moving through stiff networks and for magnetically driven helical bodies swimmers through gels whose mesh size is roughly the same size as the swimmer (86; **Figure 5*b*,*c***). Some organisms even alter the physics of their environment through chemical processes to improve their mobility. Urease enzyme released by the pathogen *Helicobacter pylori* modulates the fluid's local pH but also reduces mucin viscoelasticity, allowing the bacteria to penetrate a mucus lining protecting the gut (87; **Figure 5*d***).

2.2.4. Anisotropic fluids. Our last example of a Type II system is swimming in an anisotropic medium that relaxes toward orientational order. Network formation in mucus can lead to such order (90) and may be relevant to spermatozoa navigation through the cervical canal (**Figure 5*a***; 88). A model fluid used to investigate such environments, both experimentally and theoretically, is a liquid crystal. The standard models and fluids used, like the bacteria-friendly lyotropic chromonic disodium cromoglycate (DSCG), are composed of symmetric rodlike molecules, resulting in ordered nematic phases upon cooling, and randomly oriented isotropic phases above a critical temperature. Near the phase transition, the motion of a *Bacillus subtilis* cell through the environment can temporarily melt the liquid crystal, leaving an alluring helical trail in its flagellar wake (**Figure 6*a***; 91).

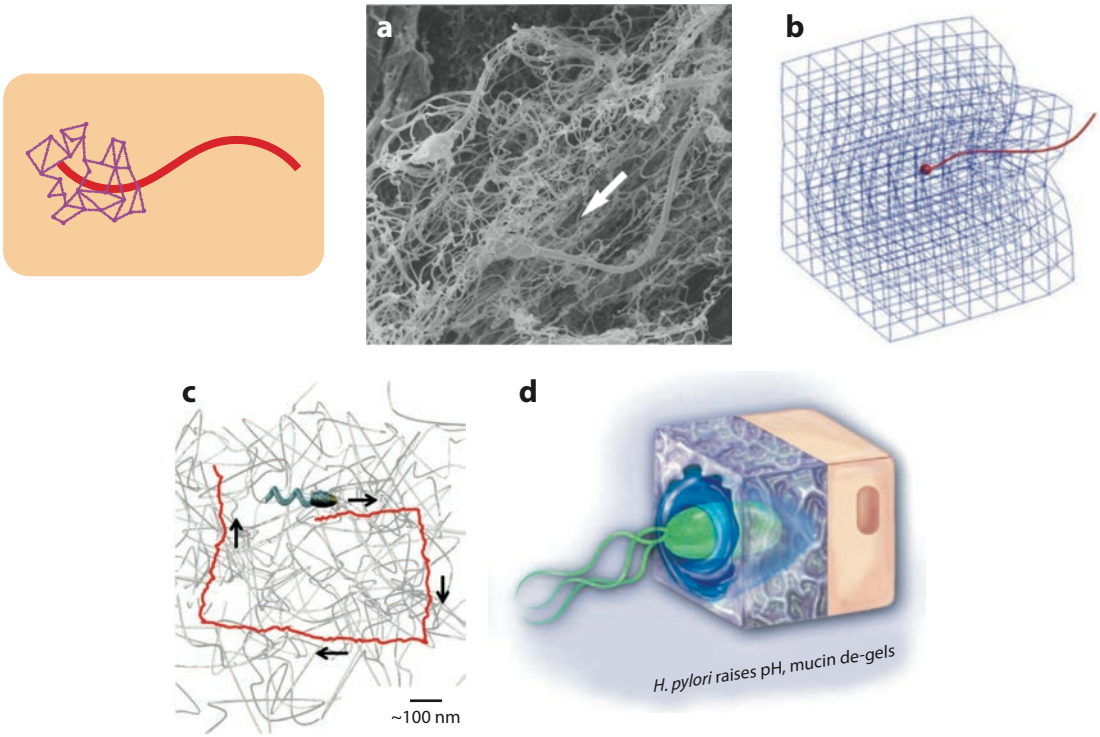

Figure 5

Type II systems: networks and gels. (*a*) Spermatozoa swim in the direction of the arrow through the anisotropic glycoproteic meshwork in cervical mucus. Panel adapted with permission from Reference 88. (*b*) An undulating body swims faster through a stiff elastic network. Panel adapted with permission from Reference 89. (*c*) A magnetically driven synthetic swimmer probes a gel. Panel adapted with permission from Reference 86. (*d*) *Helicobacter pylori* chemically alters the rheology of its environment, improving its mobility. Panel adapted from Reference 87.

The details of swimming in a liquid crystal can depend strongly on another feature not present in many other complex fluids, a surface anchoring energy, that penalizes departures from a given molecular orientation there due to surface chemistry. The continuum director field describing the orientation of (stacked) DSCG molecules, for example, preferentially anchors to biological membranes in the tangent plane (92). As a consequence, when elongated bacteria are placed in such fluids, they tend to align with the local director field—the elastic energy in the bulk liquid crystal is smaller when the body is more streamlined. Exploiting this observation, director-guided motion is seen along the surface of nematic tactoids (**Figure 6*b***; 92) and has been used to trace a long path for cargo-carrying *Proteus mirabilis* cells to follow (93; **Figure 6*c*,*d***). Liquid crystal director fields are also bound by topological constraints, which generically result in the presence of defects, points at which the director field is nondifferentiable (98). Different defects induce different bacterial behavior; $+1/2$ defects encourage accumulation, whereas $-1/2$ defects (**Figure 6*e***) result in mean depletion (94, 99).

Theoretical perspectives on swimming in anisotropic fluids are stymied by a dramatic coupling of nonlinearities and an avalanche of dimensionless groups, but asymptotic analysis in some simplified settings has provided some insight. The predictions that have emerged are surprising; for instance, an infinite swimming sheet can swim either with or against the direction of its wave propagation. The direction depends on the rotational viscosity, which determines the

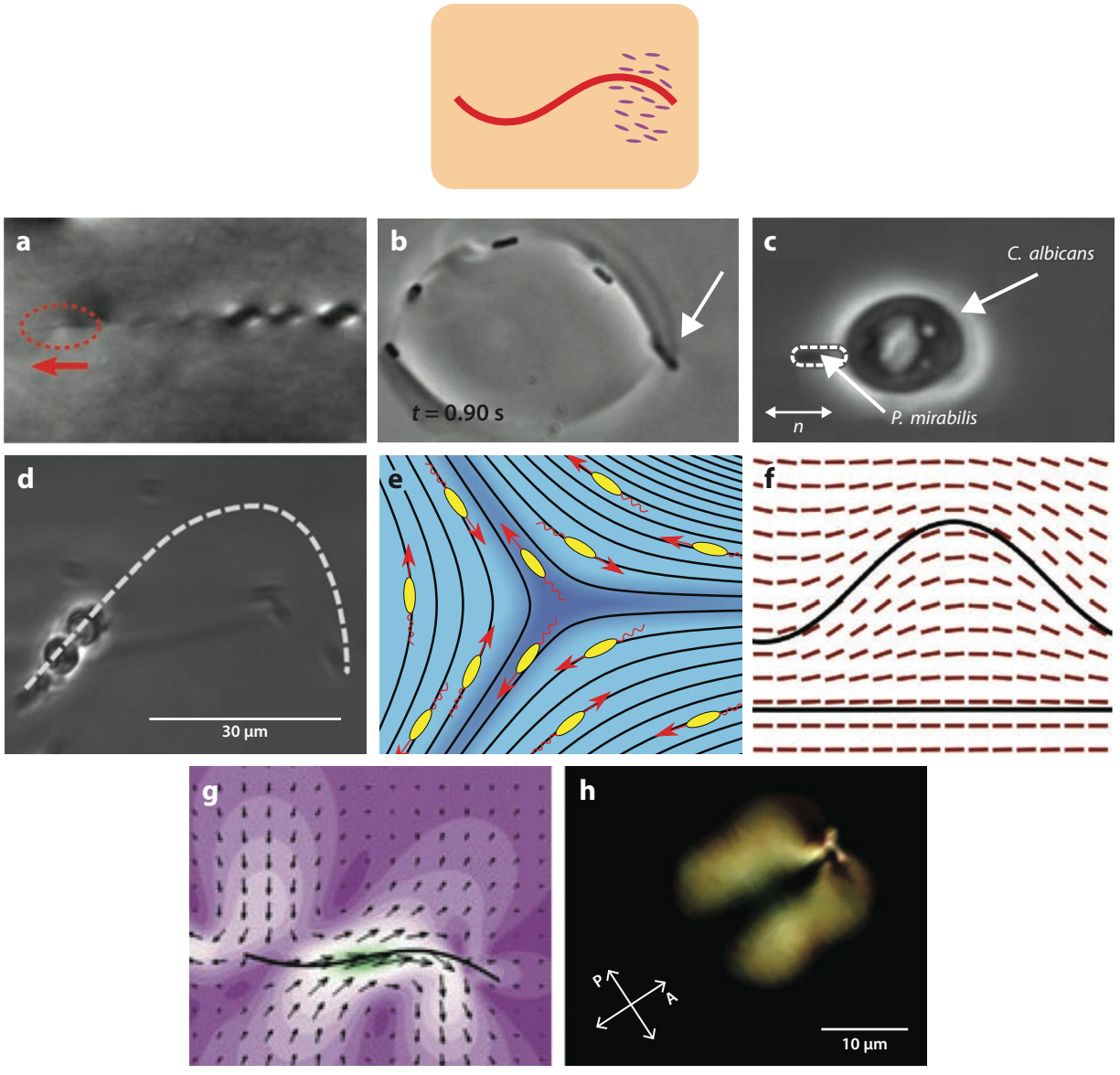

Figure 6

Type II systems: anisotropic fluids. (*a*) Nematic-biphasic melting in the wake of a small *Bacillus subtilis* cell (highlighted by the *dotted red oval*) that is swimming to the left. Panel adapted from Reference 91. (*b*,*c*,*d*) *Proteus mirabilis* in director-guided motion (*b*) near a nematic tactoid, with a cell indicated by an arrow (panel adapted with permission from Reference 92), and pushing (*c*) a large yeast cell and (*d*) two microbeads along prescribed paths (panels *c* and *d* adapted from Reference 93). (*e*) Depletion of bacteria near a −1/2 topological defect. Panel adapted with permission from Reference 94 (CC BY 4.0). (*f*,*g*) Director field (*f*) near a waving sheet and an infinite wall in a liquid crystal with strong tangential anchoring conditions (panel adapted with permission from Reference 95) and (*g*) around a finite body, with velocity field (and magnitude, *colored*; panel adapted with permission from Reference 96). (*h*) A self-propelling liquid-crystal droplet swims through a bulk nematic phase, viewed by optical micrograph. Arrows indicate the orientations of the polarizer (P) and analyzer (A). Panel adapted with permission from Reference 97.

rate at which the fluid's orientational order is recovered and, thus, the rate at which an elastically generated backflow is produced (33, 95). As in the case of isotropic viscoelastic fluids, the bulk elasticity can play the role of effective confinement, leading to increased swimming speeds. The degree to which the director field may be deformed is characterized by the Ericksen number, $\mathrm{Er} = \mu UL/K$, a ratio of the viscous-to-elastic forces in a flow, where μ is the fluid viscosity, U and L are characteristic velocity and length scales, respectively, and K is a bulk elastic modulus (a Frank elastic constant; 98). Here again, choosing $T_{\mathrm{obs}} = \mu L^2/K$ as an elastic relaxation timescale, and $T_{\mathrm{swim}} = L/U$ a swimming timescale, the Ericksen number $\mathrm{Er} = T_{\mathrm{obs}}/T_{\mathrm{swim}}$ is the Weissenberg number in different clothing (or the Deborah number in the oscillatory setting).

The constituents of a liquid crystal generally have a preferred orientation on a given surface, and a surface anchoring energy represents the cost of deviation from this configuration there—large anchoring strengths can distort the field well into the bulk (98). **Figure 6*f*** shows the director field of a nematic liquid crystal around an infinite sheet swimming near a flat surface at small Ericksen number, with strong tangential anchoring on both boundaries. Although the rotational viscosity and backflow can alter the swimming direction, its effects are substantially magnified when the anchoring strength is large (95). Simulations of finite-length swimming sheets show similar results but also reveal that the director field deformations and associated elastic stresses, like for swimmers in viscoelastic fluids, are largest near the tail (**Figure 6*g***; 96).

Our last example blurs the lines between Type II and Type IV systems. A liquid crystal droplet can swim through a bulk nematic phase due to initial symmetry breaking by Marangoni stresses on the surface, with coherent motion supported by orientation-dependent van der Waals forces at the boundary (**Figure 6*b***; 97). As is generally the case for swimming in anisotropic environments, the swimming direction is biased into the direction of the background director field.

2.3. Small De, Large Bn, Small ϕ: A Single Swimmer Near a Large Rigid Obstacle (Type III)

> There was a soggy collision of a bacterial rod with the ship. The substance of the bacterium bent about the curve of the window, sprang back into shape and bounced off, leaving a smear that washed off slowly.
>
> —*Fantastic Voyage* by Isaac Asimov (Reference 17)

Type III represents systems with a single swimmer in a Newtonian fluid near a rigid obstacle. Depending on the Benes number, the obstacle geometry may come into view. Many features of swimming near obstacles, however, are informed by the limit of infinite Benes number (e.g., swimming near an infinite wall).

2.3.1. Swimming near a wall. For very large Benes number the obstacle may appear to the swimmer as a flat wall. One early theoretical study by Katz placed Taylor's infinite swimming sheet model with fixed gait near a rigid boundary (100). The swimming speed was found to increase dramatically as the body neared the wall but with greater energetic cost. This fact has been used to rationalize swimming enhancement when complex fluid stresses produce effective confinement, as we have already seen in some Type II systems.

More complex body dynamics and trajectories also appear when a boundary is nearby, including surface accumulation (101) and circular orbits (**Figure 7*a*,*b***; 103, 114–116). *Chlamydomonas* algae cells scatter from a wall at an angle determined by their flagellar geometry (**Figure 7*c***; 104, 117), and the random tumbling of *Escherichia coli* is suppressed near surfaces owing to increased hydrodynamic resistance (118, 119). Hydrodynamic effects can be substantial; metallic synthetic swimmers can even swim upward against gravity using the hydrodynamic interaction with a wall (**Figure 7*d***) (105). Surface accumulation may also be a statement of mean behavior, with individual swimmers undergoing periodic departure and return (110, 120).

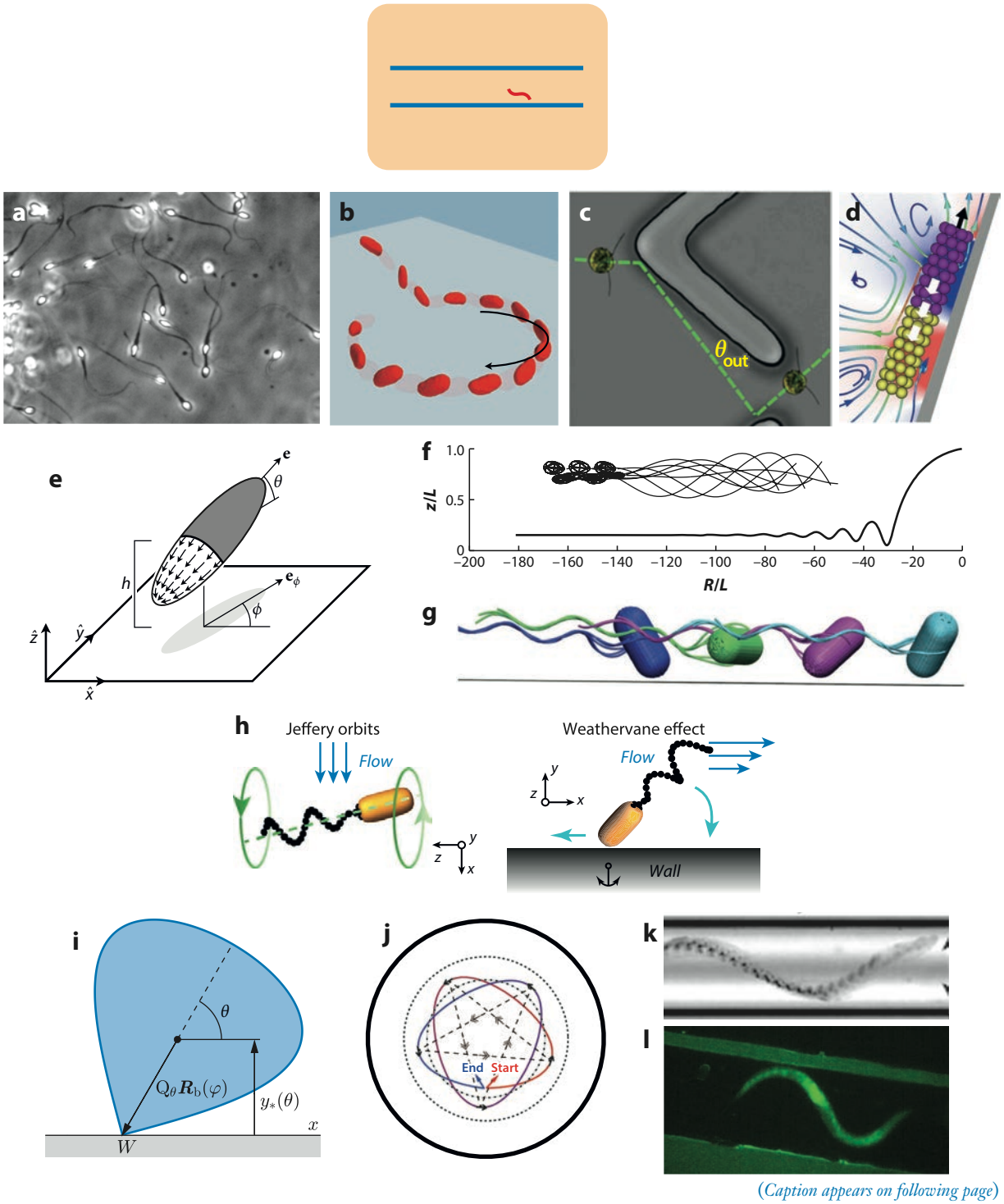

(*Caption appears on following page*)

Figure 7 (*Figure appears on preceding page*)

Type III systems: a single swimmer near a large rigid obstacle (swimming near a wall). (*a*) Surface accumulation of spermatozoa. Panel adapted with permission from Reference 102. (*b*) Holographic recovery of circular swimming of an *Escherichia coli* cell. Panel adapted from Reference 103 (CC BY 4.0). (*c*) A *Chlamydomonas* cell departs from a wall at an angle related to its flagellar geometry. Panel adapted from Reference 104. (*d*) Swimming up a wall against gravity. Panel adapted with permission from Reference 105. (*e*) Far-field models are often adequately predictive (panel adapted with permission from Reference 106), but more detailed simulations can resolve the role of cell shape and deforming bodies, for (*f*) dynamic accumulation of spermatozoan swimming (panel adapted with permission from Reference 107) and (*g*) wobbling of multiflagellated cells (panel adapted with permission from Reference 108). (*h*) A "weathervane effect" due to a background flow can result in upstream swimming. Panel adapted from Reference 109 (CC BY 4.0). (*i*) Body shape can strongly affect near-wall scattering and statistics. Panel adapted with permission from Reference 110. (*j*) Confinement-induced periodic trajectories of a model swimmer. Panel adapted with permission from Reference 111. (*k*) A confined *Paramecium* cell swims with a helical trajectory. Panel adapted with permission from Reference 112. (*l*) *Caenorhabditis elegans* combines swimming and crawling motions under confinement. Panel adapted with permission from Reference 113.

Modeling and simulation have been used to better understand the extent to which hydrodynamics alone can describe these phenomena. Far-field hydrodynamics captures many features robustly. The model Janus swimmer in **Figure 7*e*** was used to explore the accuracy of such theories, showing them to be remarkably accurate down even to swimmer-wall distances well below the swimmer length (106, 121). But to understand the interplay between flagellar beating and surface interactions requires more detailed flagellum-resolving simulations like those shown in **Figure 7*f*,*g*** (107, 108, 122–125). The combination of wall effects and a background flow can encourage an unexpected upstream swimming due to a weathervane effect (**Figure 7*h***; 109, 126–128). Body geometry and fluctuations can also strongly affect orientational statistics (124, 129–131), as elegantly explored in configuration space by Chen & Thiffeault with the asymmetric model swimmers shown in **Figure 7*i*** (110). Other alluring trajectories abound, including periodic dynamics under confinement of model swimmers (**Figure 7*j***; 111, 132–135) and in experiments with a *Paramecium* cell (**Figure 7*k***; 112).

Helical bodies in cylindrical confinement enjoy a similar speed enhancement as that described by Katz, though the details depend on the helical geometry and distance to the boundary (52, 136). The optimal pitch angle for self-propulsion is similarly affected. The compliance of the cell and particularly any thin, highly deformable motility organelles can thus strongly affect both swimming speeds and energetic costs (137). Larger slender bodies like *C. elegans* also deform under confinement (**Figure 7*l***), and their motility is affected accordingly (113, 138).

2.3.2. Geometric obstacles. As the Benes number decreases the obstacle shape begins to come into view [Bn = $O(1)$ when the body and obstacle are roughly the same size]. Billiard-like motion, intermittent periods of entrapped orbiting states, and randomized escape behavior are observed in a fluid with finite-sized obstacles in both synthetic and living systems (**Figure 8*a*,*b***; 139, 140). The far-field flow generated by a non-Brownian pusher-type swimmer (a dipolar swimmer that expels fluid along its swimming direction and draws it in laterally) near a spherical obstacle suggests hydrodynamic entrapment above a critical Benes number that depends on the dipole strength. **Figure 8*c*** shows the trajectories of pushers swimming toward colloids of varying sizes relative to the swimmer size, showing a nonmonotonic scattering angle with increasing colloid size and hydrodynamic entrapment by the largest obstacle (141). With the inclusion of thermal fluctuations, trapping time statistics depend most notably on the rotational diffusivity of the swimmer. A puller-type swimmer (which instead draws fluid inward along its swimming direction and expels it laterally) can pull itself into an entrapped state near much smaller obstacles.

If entrapment does not occur or is only temporary, the interaction can still affect the long-time statistics. Such scattering events can enhance transport even at low obstacle densities (**Figure 8*d***; 142). The mechanism of self-propulsion (141, 149–152) and obstacle shape (143, 153), for instance,

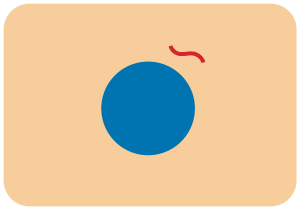

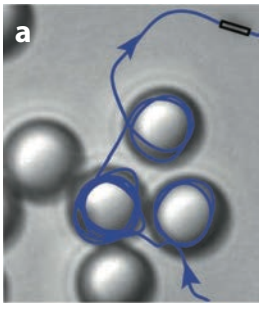

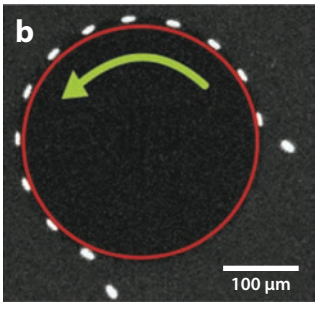

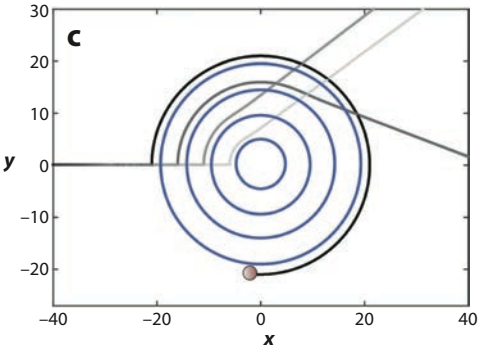

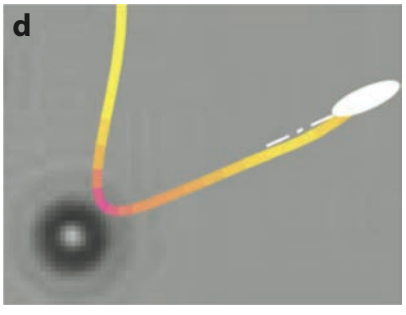

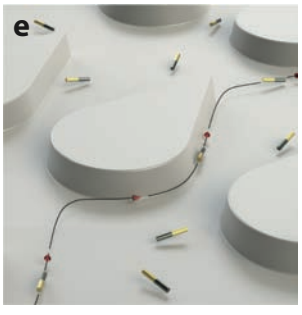

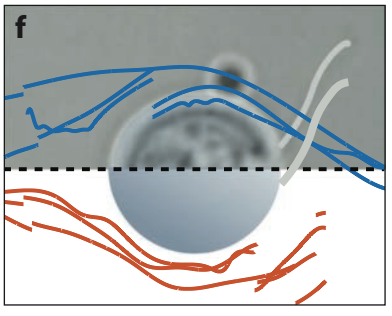

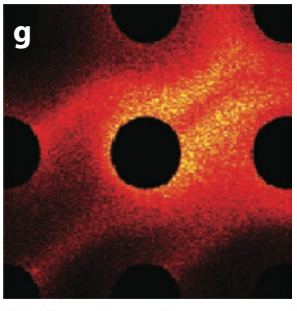

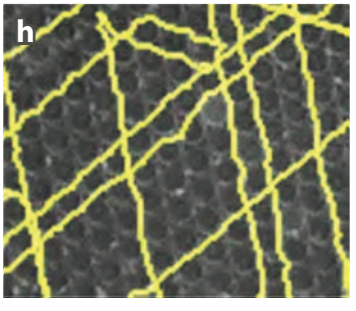

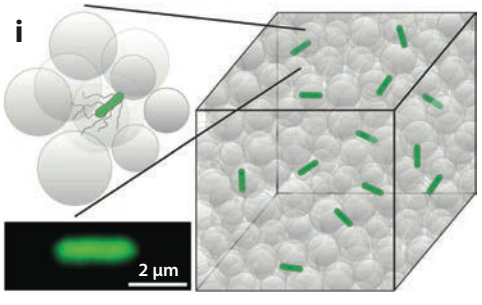

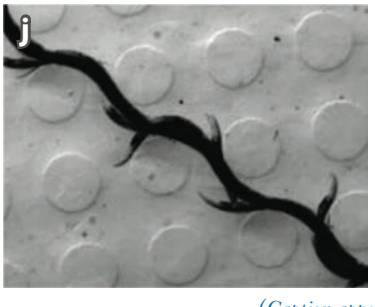

(*Caption appears on following page*)

Figure 8 (*Figure appears on preceding page*)

Type III systems: geometric obstacles. (*a*,*b*) Scattering and entrapment (*a*) of synthetic swimmers by spherical colloids (panel adapted with permission from Reference 139) and (*b*) of *Escherichia coli* cells by cylindrical posts, where the arrow indicates the direction of swimming motion (panel adapted with permission from Reference 140). (*c*) Trajectories of pusher-type swimmers around colloids of four different sizes. Scattering is nonmonotonic in the colloid size, whereas entrapment is predicted above a critical Benes number (e.g., colloid size) that depends on the dipole strength and swimmer diffusivity. Panel adapted with permission from Reference 141. (*d*) Cell transport may be enhanced due to scattering events even at low obstacle density. Panel adapted from Reference 142 (CC BY 4.0). (*e*) Scattering may be guided by obstacle shape. Panel adapted with permission from Reference 143. (*f*) Entrainment of small obstacles depends on their size and the mechanism of propulsion. Panel adapted with permission from Reference 144. (*g*) A simulated cloud of noninteracting swimmers spreading through a periodic array of posts. Panel adapted with permission from Reference 145. (*h*,*i*) Repeated surface interactions in porous media can (*h*) focus swimming trajectories [panel adapted from Reference 146 (CC BY 3.0)] or (*i*) result in effective diffusion [panel adapted from Reference 147 (CC BY 4.0)]. (*j*) *Caenorhabditis elegans* transitions from swimming to crawling in a structured environment to enhance mobility. Panel adapted with permission from Reference 148.

the teardrop-shaped obstacles shown in **Figure 8*e***, can also strongly affect the interaction with and departure from the surface. Sorting and rectification devices meant to exploit such interactions have been constructed and explored, including funnels and gears (16).

For smaller obstacles it becomes more important whether or not they are fixed in space or free to become entrained by a passing swimmer. If entrained, the shape and stroke of the swimmer become particularly important (**Figure 8*f***; 144, 154). Transport of yet smaller obstacles, or even fluid particles, return us closer to Type I problems and the general question of fluid entrainment by swimming bodies (155). The Benes-number dependence on entrapment and particle entrainment was performed by Shum & Yeomans (156), and a generic enhancement of swimming by the reduction of wobbling in colloidal suspensions was explored by Kander et al. (157).

There may instead be many large obstacles to navigate, and the dynamics described above may take place over repeated interactions. **Figure 8*g*** shows a simulated cloud of active Brownian swimmers spreading in a periodic array of posts. Generic features in such systems include boundary layers and thin regions of increased swimmer concentration in the wake of an obstacle (145). In systems with more tightly packed obstacles, synthetic swimming particles can hop from colloid to colloid with a trapping time that depends on fuel concentration, whereas *E. coli* trajectories are rectified into long, straight runs (**Figure 8*b***; 146). The uncertainty in trapping times and exit orientations leaving one obstacle leads to an effective diffusion through a bulk porous medium (**Figure 8*i***; 147). In this example, depending on whether the obstacle size is chosen to be the size of the colloid, roughly 10 μm, or the narrow pore size between obstacles, 10^{-1} μm, the Benes number ranges from 10^{-2} to 1.

As usual, body deformability can be important. *C. elegans*, for instance, transitions from swimming to crawling motion to enhance its mobility in a structured environment. **Figure 8*j*** shows this nematode traversing a periodic array of obstacles. When Bn is of order 1, particularly if the undulatory wavelength is the same size as the obstacles, the swimming is focused into straight trajectories like the *E. coli* cells in **Figure 8*b*** as the body pushes off each obstacle one after another (148, 158).

2.4. Large De, Large Bn, Small ϕ: A Single Swimmer Near a Deformable Obstacle (Type IV)

> The white cell was tremendous. It was five times as large in diameter as the *Proteus*, perhaps larger; a mountain of milky, skinless, pulsing protoplasm in comparison to the individuals watching.
>
> —*Fantastic Voyage* by Isaac Asimov (Reference 17)

In Type IV systems, a large obstruction relaxes on a timescale longer than or commensurate with that of a single organism's motion. Examples include air–water interfaces, oil–water interfaces

(159), thin films (160), and mucus-lined tissues like those found in the mammalian reproductive tract (36). Even if the action of a swimmer is insufficient to drive substantial normal surface deformations, the freedom of tangential interface motion can affect swimming behaviors. For example, the orientation of the circular swimming patterns of organisms like *E. coli* are reversed relative to what is observed for swimming near a rigid wall (**Figure 9*a***; 161, 162, 168, 169). This change in observed behavior can be rationalized by examining the hydrodynamics of swimming with a mirror image across the interface (**Figure 9*b***; 106, 162, 168, 170, 171). But the behavior can also be very sensitive to the surface adsorption of organic materials and surfactants, which can render the surface more or less rigid (161).

Surface absorption of the swimmer is possible as well, which can lead to distinct trajectories depending on the nature of the trapped state. **Figure 9*c*** shows numerous trajectories of *Pseudomonas aeruginosa* cells at an oil–water interface, which include diffusive paths, curved trajectories, and rapid pirouette rotations (163). The tangential flows and resultant swimmer dynamics generally depend on the relative obstacle size or interfacial confinement and the common possibility that surfactants are present on the interface (**Figure 9*d***; 164, 172). Surfactants can rigidify the interface and nudge the system back toward Type III interactions of a swimmer with a rigid obstacle or wall (173, 174).

Stronger swimmers, or softer boundaries, can result in normal surface deformations as well. Many theoretical techniques have been used to probe this problem including far-field approximations (**Figure 9*e***; 175), a conformal mapping approach (165), and small amplitude asymptotic analysis for swimming sheets (**Figure 9*f***; 166) and squirmers (176). Depending on the nature of the swimmer and the surface physics, the deformability of the boundary can result in either enhancement or retardation of swimming speeds for a given swimming kinematics (**Figure 9*g***; 166, 167). Even tighter confinement can lead to even more dramatic boundary and swimmer shape deformations. A model amoeboid swimming through a narrow compliant channel, for instance, undergoes a marked decrease in swimming speeds as the channel narrows (177, 178).

2.5. Small De, Small Bn, Large ϕ: Many Swimmers in a Suspension of Small Rigid Obstacles (Type V)

Type V systems feature environments with small rigid obstacles, as in Type I, but with a sufficiently large swimmer concentration ϕ so that swimmer interactions become relevant. With small Bn, the fluid is again reasonably approximated as a continuum medium at the scale of the swimmers. A first step in the direction of understanding large swimmer concentrations is to consider the interactions of two swimmers. When two swimmers approach each other the details of their shapes and swimming cycles come into view. For example, waving sheets and filaments can be synchronized through hydrodynamic interactions—**Figure 10*a*** shows two nearby swimming spermatozoa swimming in synchrony (179). But hydrodynamic interactions are not always dominant in such settings. The synchronization of *C. elegans* nematodes, for instance, is based more on the effects of steric hindrance (**Figure 10*b*,*c***; 180).

The collective dynamics of many swimmers, meanwhile, remains a particularly vibrant research area that has been treated to excellent and deeper treatments beyond the scope of this review (4, 188–193). Among the main features observed in these systems, the long-range nature of hydrodynamic interactions in viscous fluids can result in positional and orientational correlations among groups of swimmers even at volume fractions as low as $\phi = 1$–2% (181, 194). Such correlations can depend on body shape—rotation and alignment are different for sphere-like and rod-like bodies (28). At large swimmer concentrations, new complex phenomena begin to emerge. Swimmer interactions can lead to increases in effective velocity and diffusion. For example, **Figure 10*d*** shows a suspension of *B. subtilis* cells, each roughly 4 μm long, with structures observed on the

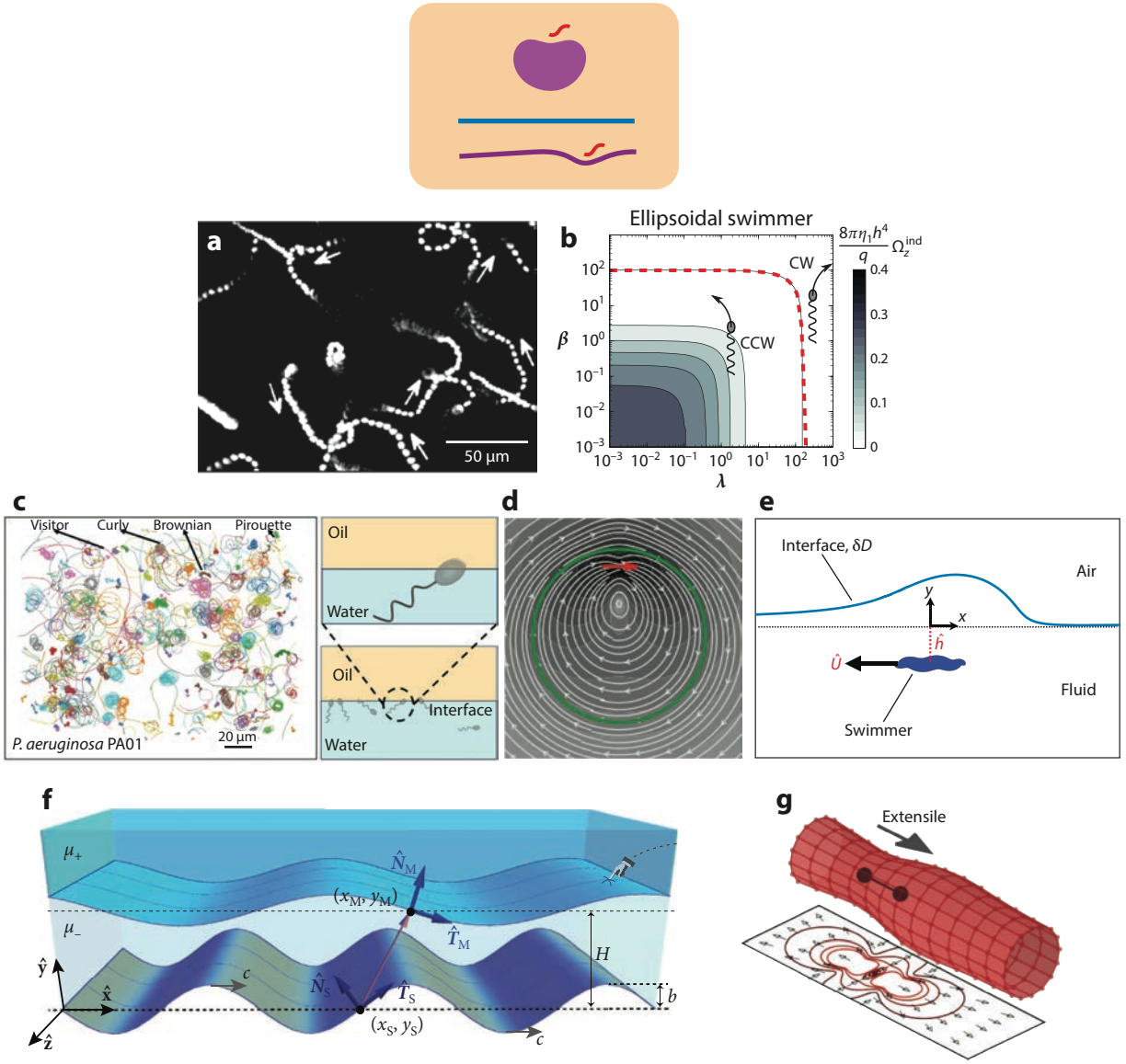

Figure 9

Type IV systems: a single swimmer near a deformable obstacle. (*a*) Counterclockwise circular trajectories of *Caulobacter crescentus* cells (*arrows* denote swimming directions) at an air–water interface. Panel adapted with permission from Reference 161. (*b*) Purely hydrodynamic arguments show similar counterclockwise (CCW, free surface) to clockwise (CW, solid wall) rotations depending on the viscosity ratio λ and the surface viscosity β (*contours* of the rotation rate are shown). Panel adapted with permission from Reference 162. (*c*) Free and adhered states of *Pseudomonas aeruginosa* cells at an oil–water interface—distinct trajectories (*left*) are due to differing trapped states (*right*). Panel adapted with permission from Reference 163. (*d*) Flows in and along the surface of a confining droplet (denoted by the *green boundary*) due to an interior point force (denoted by the *red arrow*). Panel adapted from Reference 164 (CC BY 4.0). (*e*) Normal surface deformations may be generated by distant swimmers. Panel adapted with permission from Reference 165. (*f*) Closer swimmers can deform an interface more substantially, resulting in stronger speed and efficiency adjustments. Panel adapted with permission from Reference 166. (*g*) Soft confinement can either increase or decrease the speed of model swimmers. Panel adapted with permission from Reference 167.

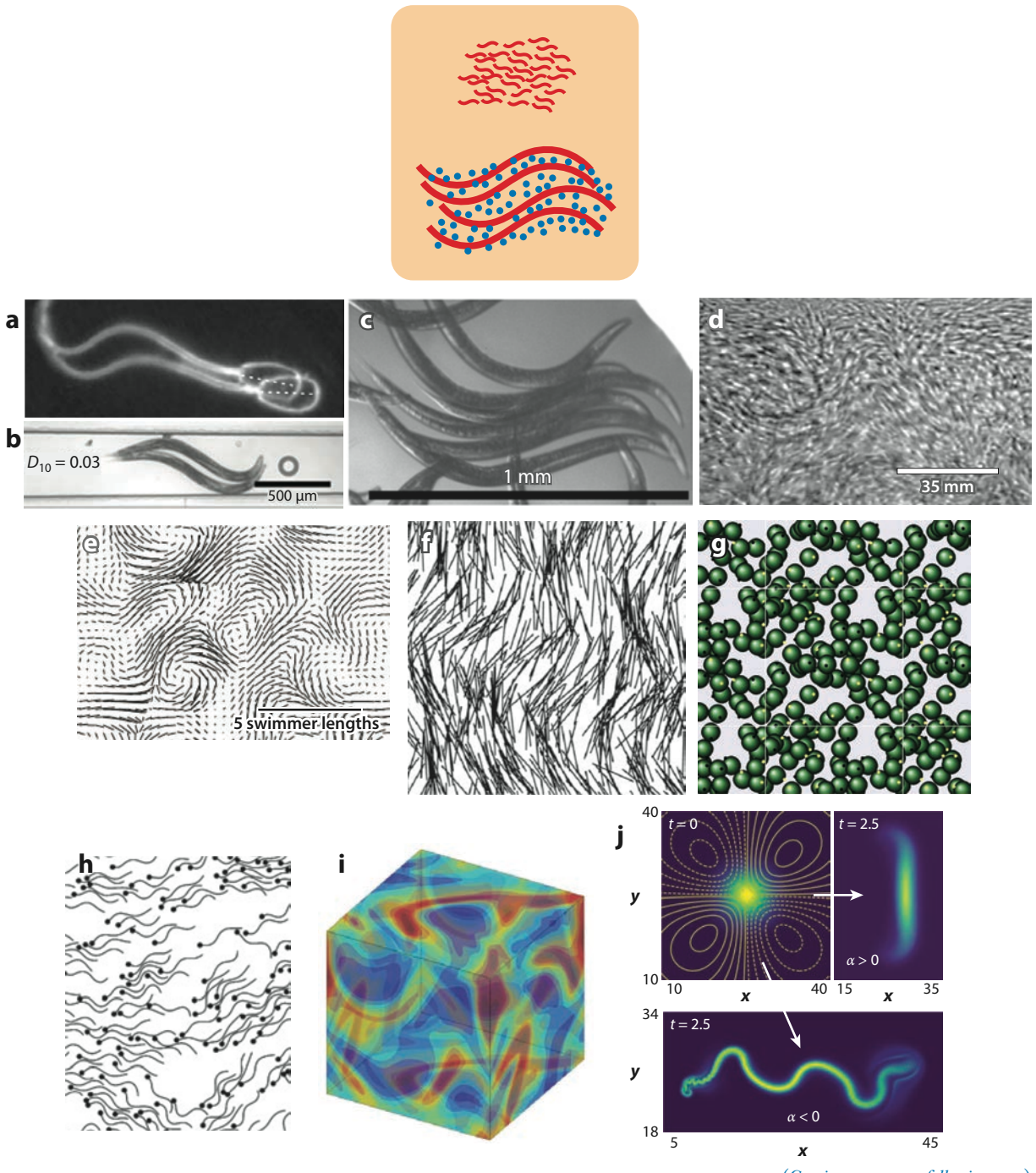

(*Caption appears on following page*)

Figure 10 (*Figure appears on preceding page*)

Type V systems: many swimmers in a suspension of small rigid obstacles. (*a–c*) Synchronization of (*a*) swimming spermatozoa (panel adapted with permission from Reference 179) and (*b*,*c*) *Caenorhabditis elegans* (panels adapted from Reference 180). (*d*) Collective motion of *Bacillus subtilis* cells shows correlations on much larger scales than the individual swimmer size. Panel adapted with permission from Reference 181. (*e*) Velocity field from collective simulations resolving individual swimmers. Panel adapted with permission from Reference 182. (*f*) Onset of an orientational instability in a suspension of nearly aligned "pusher" swimmers. Panel adapted with permission from Reference 183. (*g*) Collective motion of model spherical squirmers. Panel adapted with permission from Reference 184. (*h*) Synchronization and aggregation within large groups of model spermatozoa. Panel adapted from Reference 185 (CC BY 4.0). (*i*) Swimmer concentration field via solution of moment equations in a coarse-grained theory. Panel adapted with permission from Reference 186. (*j*) Self-stretching of a Gaussian concentration of rightward-pointing swimmers, along the swimming direction and unstable for pushers ($\alpha < 0$) or transverse to the swimming direction for pullers ($\alpha > 0$). Panel adapted with permission from Reference 187.

larger scale of the 35-μm bar shown at the bottom right (181). These structures lead to enhanced diffusion of tracer particles that depend on their size (195) and shape (196). Interactions among externally driven rotating bodies can result in clustering, colony-scale rotations, and odd viscosity (197–199). Such dynamics have also been observed in swimming suspensions of *Thiovulum majus* bacteria cells (200) and starfish embryos (201).

2.5.1. Simulations and theoretical advances. A number of agent-based simulations have been used to explore the mechanisms causing the group behavior. Hernandez-Ortiz et al. (182) showed that the type of swimming (either pushed from the back or pulled from the front) changes the hydrodynamic interactions and thereby the large-scale group behavior. As in experiments, the velocity field shown in **Figure 10*e*** shows correlated motion on a scale much larger than the individual swimmer size; the included scale bar is five swimmers long. A generic feature in active suspensions for small ϕ is the emergence of long-range orientational order for pusher-type swimmers, seen, for instance, in simulations of many pusher-type swimming rods (**Figure 10*f***; 183). Such group behavior is found in simulations using spherical squirmers as well (**Figure 10*g***; 184). In this system, at higher swimmer concentrations the isotropic state destabilizes and relaxes into polar order for both pushers and pullers, unlike in dilute theories for which only isotropic suspensions of pushers are orientationally unstable.

These agent-based simulation models have quantified how hydrodynamic interactions and swimmer shape impact swimmer velocity and orientational correlations (183, 202–206). They have also used passive tracer particles that are advected and mixed by the flows created by the swimmers as a method to quantify collective behavior (207–209). Within large groups, clustering is observed, and is attributed to steric and hydrodynamic pairwise interactions similar to those seen in dilute suspensions (**Figure 10*b***; 185). Such results highlight one feature that is just starting to be explored: how the details of swimmer shapes and strokes affect short-range correlations within systems that show large-scale group dynamics (210, 211).

Theoretical advances have involved the derivation and analysis of continuum field equations for the coarse-grained system dynamics (192). Further simplification is found through closure approximations, generating coupled equations for the first few local orientational moments, which produce results similar to those found in full agent-based simulations. **Figure 10*i*** shows spatial variations in a concentration of pushers that have emerged out of an isotropic state using the Saintillan–Shelley model equations (186). The self-stretching of localized colonies, and a cascade of transverse instabilities in thin concentration bands, provides insight on these more fully developed global dynamics (**Figure 10*j***; 187, 212). Recently, field theories that include fluctuations and correlations have been developed to examine the onset of collective behavior (209, 213, 214).

2.5.2. Complex rheology. The activity and orientational order that emerges in active systems can confer the solvent-suspension system with features normally associated with bulk complex

fluids. The effective viscosity of fluid containing puller-type swimmers, specifically *Chlamydomonas reinhardtii*, has been found to increase on account of their swimming activity (215, 216). Suspensions of pusher-type swimmers like *B. subtilis* (14) and *E. coli* (217–219), meanwhile, are found to decrease the effective viscosity of the medium. These generic effects of extensile (pusher) and contractile (puller) suspensions are also recovered theoretically (11, 220). As the swimmer volume fraction increases, the decreased viscosity for suspensions of pusher-type swimmers can reach zero, effectively a superfluid state, where the medium can be sheared with no stress, and then into negative effective viscosity, where work must in fact be done to keep the medium from shearing itself (11–15). The superfluid response can also cause shear-banding in the velocity profile (221).

These suspensions are often found to have a swimmer contribution that decreases with background shear rate, as the active stresses that they produce become drowned out by the large-scale motion. Many models have computed the contribution to rheological properties from the hydrodynamic disturbance caused by the swimmers. These models show a decrease due to shear-induced swimmer alignment, much like the shear-thinning found in suspensions of passive rods. There is also a diffusive contribution, which can lead to non-Newtonian behavior of the suspension (222).

Suspensions of spherical squirmers have been used to explore the rheology of very high swimmer concentrations, where the lubricating region between individual swimmers dominates their interactions. The effective shear viscosity is found to increase for both pushers and pullers compared to a similar suspension of inert spheres. But for bottom-heavy squirmers the distinction between pushers and pullers returns, and viscosity reductions down to superfluidity appear again for pusher suspensions (223).

The role of body deformability on active suspensions and their effective rheology remains a generically open area of inquiry, but simulations have revealed that the sign of the effective medium's second normal stress differences depends on body stiffness (224). Other non-Newtonian features due to active suspensions like viscoelasticity (11, 220, 225, 226) and yield-stress behavior (227, 228) have also been predicted. The influence of surfaces described in Type III can also impact measurements of rheological properties (229). For a more detailed analysis of active suspension rheology in general, see the recent review by Saintillan (15).

Type V systems include another fairly unexplored territory: active suspensions in media with somewhat larger obstacles (though still smaller than the swimmer size). If those small stiff obstacles are free to move, they may simply alter the viscosity of the suspending fluid. But if the obstacles are fixed either through connections to each other or to the surroundings, they alter the swimmer behavior in a different way. The stiff connection allows for the dissipation of momentum, and the obstacles will generically screen long-ranged hydrodynamic interactions. Instead, short-ranged interactions can lead to large-scale patterns (230).

2.6. Large De, Small Bn, Large ϕ: Many Swimmers in a Suspension of Small Deformable Obstacles (Type VI)

> "If you damaged it, chemicals were released into the blood-stream; chemicals that attracted white cells from all the neighboring regions." "Then, for God's sake, swim!"
>
> —Dr. Duval and Agent Charles Grant, respectively, *Fantastic Voyage* by Isaac Asimov (Reference 17)

Type II systems were characterized by small obstacles with intrinsic timescales longer than or commensurate with that of a single swimming body. If there are instead many interacting swimmers in such an environment, we find ourselves in a Type VI system. The group of swimmers may be invading a shear-thinning viscoelastic solution or gel, or an anisotropic medium like mucus.

Depending on the system, the non-Newtonian bulk fluid features may have a bearing primarily on localized behaviors and interactions or may reveal structures on much longer length scales

than the swimmers themselves. The motion of each swimmer can be changed, as previously described in Type II, and in some settings these changes to individual swimming behaviors might be sufficient for understanding the effect of viscoelasticity on group behavior. But the hydrodynamic interactions may also be modified to produce a group behavior that is not simply a shift or rescaling of theories based on Newtonian fluids.

As the volume fraction of swimmers ϕ increases, the first deviation from individual swimmer dynamics occurs due to pair interactions. Viscoelastic fluids lead to enhanced clustering and synchronization in experiments with spermatozoa (**Figure 11*a***). Infinite swimming sheets synchronize in polymeric fluids much more rapidly than they do in a Newtonian fluid (**Figure 11*b***; 113, 231). Liquid crystals also alter the strength and anisotropy of pair interactions, which can result in the convergence of swimming speeds (**Figure 11*c***; 233). The interaction may depend strongly on surface anchoring conditions on the swimmers and on nearby boundaries. In some cases the liquid crystal can contribute to swimmer repulsion; in others, collisions and group swimming have been observed (**Figure 11*d***; 234).

For larger swimmer volume fractions, group behavior on length scales much greater than the individual swimmer size once again emerges as in Type V systems. Changes in the velocities within large groups have been observed experimentally. **Figure 11*e*,*f*** shows the instantaneous velocity field of a suspension of *E. coli* cells in a viscoelastic medium, and a phase diagram of ordered and disordered states across different bacterial and polymer concentrations. For sufficiently large polymer concentration a bizarre effect is observed, the onset of occasional group transport direction reversal (235). Inhibition of large-scale group behavior and an increase in swirling oscillations are attributed to an interaction between the timescale of the collective vortex flow and the timescale of elastic fluid relaxation. This example sits at the interface between Type VI and, say, Type VII, as the system behavior depends upon both confinement and bulk rheology, e.g., upon multiple obstacles on multiple scales. The question of classification in any system requires identification of the dominant contribution for the features of interest.

The earliest works to examine these effects theoretically used a continuum field theory to track the dynamics of the active particles and a continuum stress field to track the dynamics of the complex fluid (**Figure 11*g***; 236, 238, 239). A prototypical view of group behavior among pushers is as a competition between hydrodynamic interactions that lead to alignment of swimmers and noise that tries to randomize swimming directions. Because the viscous response is driving an instability to group behavior, if the fluid does not fully relax during the instability, a viscoelastic fluid produces less group behavior than would emerge in a Newtonian fluid with the same zero-shear-rate viscosity. However, because the suspended soft obstacles do contribute to the viscous response, there can be more group behavior than if the obstacles were not present.

In addition to changing fluid instabilities, viscoelastic fluids can change the nature of group behavior. This group behavior is often characterized by chaotic swirling flows. Viscoelastic stresses can break up these large swirls. This leads to intermittency similar to turbulent drag reduction; a random isotropic suspension can be unstable, leading to large-scale flows that excite viscoelastic stresses—stresses that proceed to suppress the large-scale flows. Other works modeling group behavior in viscoelastic fluids have tracked interacting swimmers within a continuum viscoelastic fluid (**Figure 11*b***; 237). Such models also show a suppression of large-scale group behavior and fluctuations in viscoelastic fluids. Alternatively, in liquid crystals with homeotropic anchoring, distortions of the director can mediate swimmer interactions and result in collective effects (234).

Some soft systems do not fully relax at long times due to cross-linking of polymers, as in a gel. These properties have the potential to alter the behavior of concentrated groups. For example, mucus gels can change the swimming and aggregation of bacteria (240). One important feature

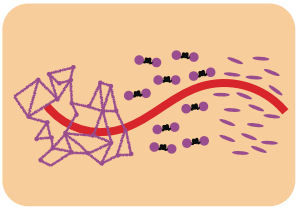

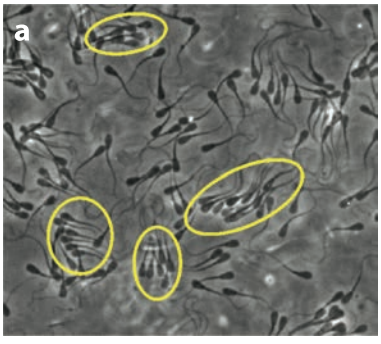

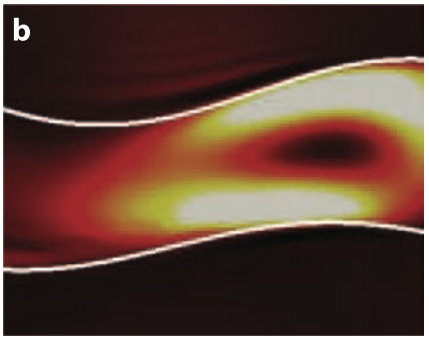

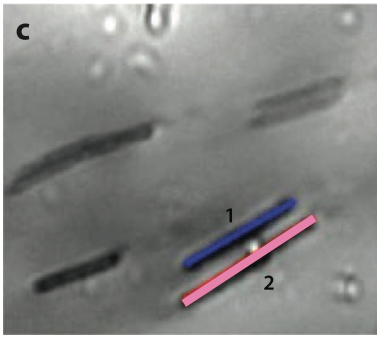

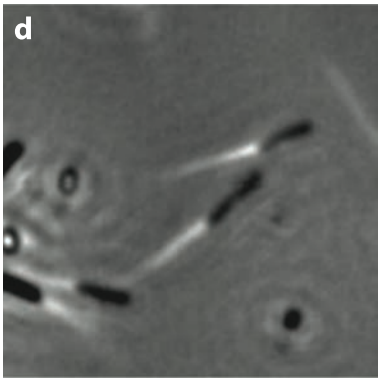

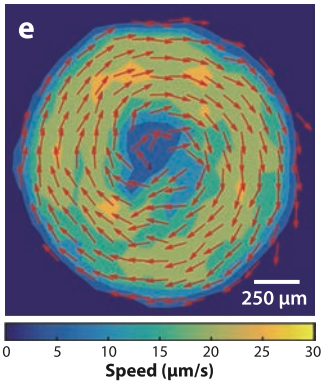

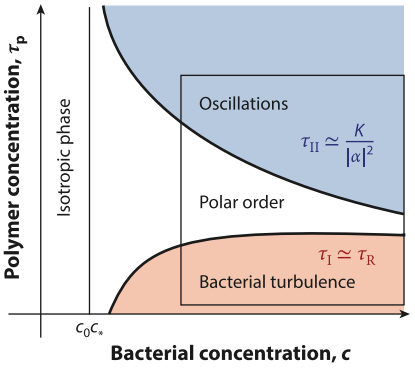

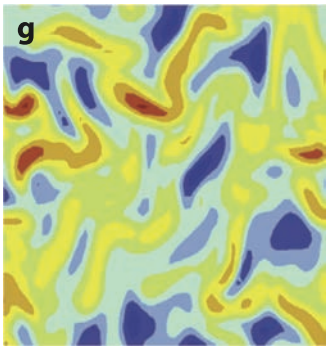

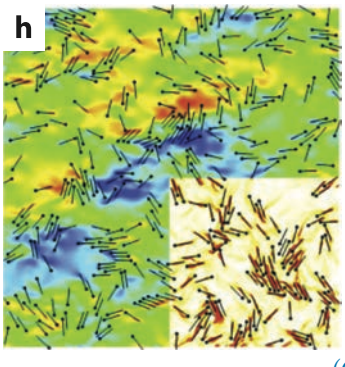

(*Caption appears on following page*)

Figure 11 (*Figure appears on preceding page*)

Type VI systems: interacting swimmers in a fluid with bulk complex features. (*a*,*b*) Viscoelasticity-enhanced synchronization (*a*) in spermatozoa, with clusters circled [panel adapted from Reference 232 (CC BY 4.0)], and (*b*) in simulations of swimming sheets (panel adapted with permission from Reference 113). (*c*) Swimming speeds of nearby *Bacillus subtilis* cells (labeled *1* and *2*) converge in an anisotropic medium. Panel adapted with permission from Reference 233. (*d*) Surface anchoring induces bacterial collision and group swimming (234). Panel adapted with permission from Reference 234. (*e*,*f*) Velocity field and magnitude of an active suspension of *Escherichia coli* cells in a viscoelastic medium and associated phase diagram of ordered and disordered states, including direction-reversing oscillations above a critical polymer concentration. Panels *e* and *f* adapted with permission from Reference 235. (*g*) Swimmer concentration from mean-field simulations of an active suspension in a viscoelastic medium reveals a reduction of large-scale structures. Panel adapted with permission from Reference 236. (*h*) Agent-based simulations show a similar reduction of large-scale structures. Panel adapted with permission from Reference 237.

of such systems is that the swimmers can change their behavior in response to the mechanical properties as well as chemical makeup of the suspending material (241).

2.7. Small De, Large Bn, Large ϕ: Many Swimmers Near a Large Rigid Obstacle (Type VII)

> "They won't bother us, I hope. Any bacteria in the circulatory system reaches a lymph node eventually. It can't negotiate the narrow twisting channels. . .". "Can we?"
>
> —Dr. Michaels and Agent Charles Grant, respectively, *Fantastic Voyage* by Isaac Asimov (Reference 17)

The collective dynamics of swimming organisms can be strongly influenced by confinement, which brings us to Type VII systems. Swimming bodies at a surface are more restricted in the orientations that they may exhibit, as seen in Type III systems with single swimmers. At the group level, such restrictions can propagate into and influence the bulk suspension organization. For example, suspensions of confined bacteria can settle into a large-scale group rotation (**Figure 12*a***; 242). When multiple rotating domains are connected by channels, the direction of bulk flow that is normally selected with equal probability may start to become influenced by neighboring domains, resulting in the possibility of ferromagnetic or antiferromagnetic global states (243). But the relationship between individual body motion and the motion of the group is not always simple. The flagellar motion of cells swimming near the boundary in **Figure 12*b*** generates a flow in the opposite direction in the bulk, so confinement simultaneously produces both upstream and downstream bacterial transport (244).

Just as in Type V systems, coarse-grained modeling has identified relationships between the geometry of confinement and the strength of the far-field hydrodynamic signal (dipole strength). The interplay between them can result in coherent rotational motion or deterioration into other classical aperiodic roiling states, or dynamic modes combining features of both (**Figure 12*c***; 192, 245, 250). Directed motion is found when the channel width is close to the length scale of rotating domains in the unbounded system (244). With even tighter confinement, phase transitions to jammed states have been found, explored using suspensions of model spherical squirmers (251).

A boundary may encourage more localized collective behavior as well. Suspensions of spermatozoa near a wall, for example, settle into an array of swimming vortices (**Figure 12*d***; 246). Although confinement can encourage the emergence or selection of collective behavior, the screening of flows by nearby boundaries can also inhibit the onset of large-scale structures. This was shown numerically in Reference 252 using a suspension of model swimmers composed of dipolar pushing beads. Screening effects may be partially offset by a stronger hydrodynamic signal; external forces or torques on immersed bodies can generate different hydrodynamic signals as viewed from afar. A suspension of active rollers, for instance, settles into smaller rolling groups

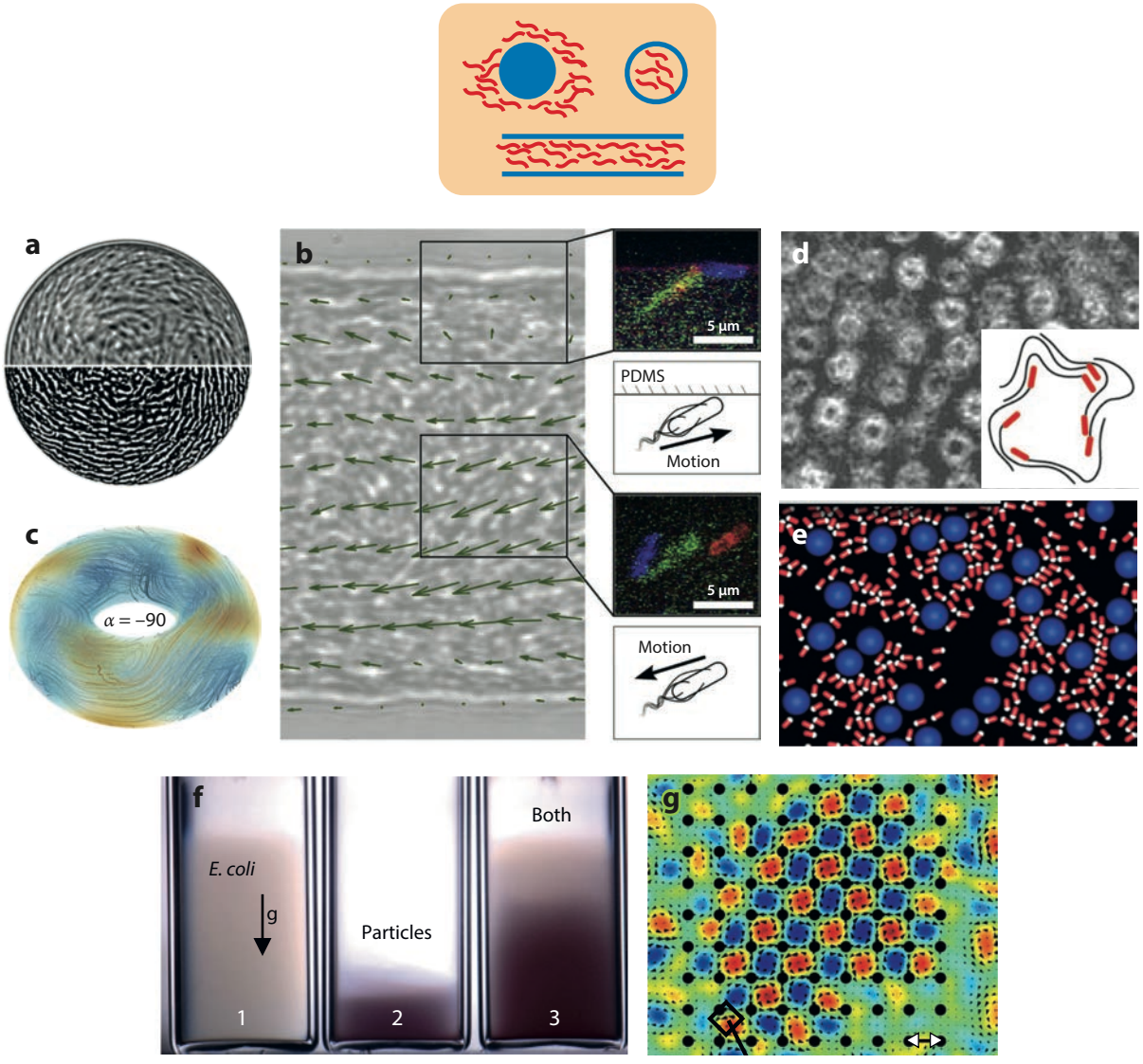

Figure 12

Type VII systems: many swimmers near a large rigid obstacle. (*a*,*b*) Edge rotation and bulk counter-rotation due to confinement (*a*) in a circular domain (panel adapted from Reference 242) and (*b*) in a racetrack, where swimmers in the bulk are carried opposite their orientation by a flow generated by swimmers at the boundary [panel adapted from Reference 244 (CC BY 3.0)]. (*c*) Confinement-induced organized swimming in three dimensions in a coarse-grained model. Panel adapted with permission from Reference 245. (*d*) Vortices of swimming spermatozoa near a flat surface. Panel adapted with permission from Reference 246. (*e*) Active particles lead to attraction among passive colloids akin to a depletion effect. Panel adapted with permission from Reference 247. (*f*) Activity by swimming *Escherichia coli* reduces the sedimentation speed of passive particles. Panel adapted with permission from Reference 248. (*g*) A lattice of bacterial vortices organized by an array of periodic obstacles. Panel adapted from Reference 249 (CC BY 4.0). Abbreviation: PDMS, polydimethylsiloxane.

due to long-ranged, wall-mediated interactions (253). If the rotations are instead about the wall normal, confinement can lead to peculiar effects such as topologically protected edge currents and colony-scale oscillations (254–258).

New features appear as the obstacles shrink in relative size to the scale of the swimmers themselves. Active particles can produce effective attraction between passive colloids similar to a depletion effect (**Figure 12*e***; 247). The sedimentation speed of passive particles can be reduced by swimming bacteria, seen in experiments with swimming *E. coli* cells and polystyrene beads (**Figure 12*f***; 248). If the obstacles are fixed in space, they can encourage the development of bacterial vortices just as was the case with external confinement (**Figure 12*g***). With certain obstacle arrangements (Kagome lattices), such obstacles can even result in net colony rotation (249).

2.8. Large De, Large Bn, Large ϕ: Many Swimmers Near a Large Deformable Obstacle (Type VIII)

In Type VIII systems the deformation of large boundaries is again substantial, to the point that they can affect the behavior of a suspension of swimming cells. We have already seen that confinement of active suspensions can encourage the emergence of a large-scale directed motion of a bulk suspension. But when the confinement is deformable, the relaxation timescale and associated surface tractions are strongly coupled to the dynamics of the suspension. Among other physical phenomena, this territory includes moving droplets of active matter.

As in Type IV systems, some of the most common deformable boundaries are fluid–air and fluid–fluid interfaces. When sufficiently many bacteria adhere to an interface, they may form biofilms, introducing to the interface elastic properties that depend on the strain of bacteria (172, 259). Bacteria on interfaces can also play an emulsion-stabilizing role similar to surfactants (260) and may render the surface viscoelastic (261). Once a biofilm is formed, the relevance of swimming diminishes, but the behavior of planktonic (freely swimming) bacteria near these surfaces can impact its spread into new territories and whether the biofilm forms at all (262). Such biofilms can disrupt natural medical function, for instance, in persistent infections like endocarditis (263), or they can be useful for applications such as bioremediation and biodegradation.

More recent advances have considered the captivating dynamics of active droplets: active suspensions with compliant, mobile confinement. Nonmotile suspensions of particles that exert an extensile stress on the surrounding fluid are known to produce large-scale flows and features similar to the swimming systems described in Type V (264). But when confined inside a droplet, the resulting interaction with the boundary can lead to geometric symmetry breaking and swimming motion (**Figure 13*a***; 265). More intricate dynamics are accessed by tuning the relative size of the droplet; an active nematic model showed periodic changes in alignment and stretching directions, resulting in zigzag trajectories (**Figure 13*b***; 266, 269). A coarse-grained model was used to reveal additional contributions of internal director field oscillations and an array of different trajectories depending on the size of the surface tension relative to the internal stress contributions (**Figure 13*c*,*d***; 267).

Active droplets present a curious question of placement for the classification system. When droplets move as a consequence of active internal stresses, what is more central, the self-transporting suspension internal to the droplet, or the net effect resulting in what appears to be a single swimmer at a much larger scale? We have included these systems in Type VIII because of the critical importance of the boundary deformability, but in this case the boundary might be considered the swimmer itself. **Figure 13*e*** shows a schematic for how Marangoni stresses on the surface of a liquid crystal droplet can couple to internal elastic modes, resulting in coherent

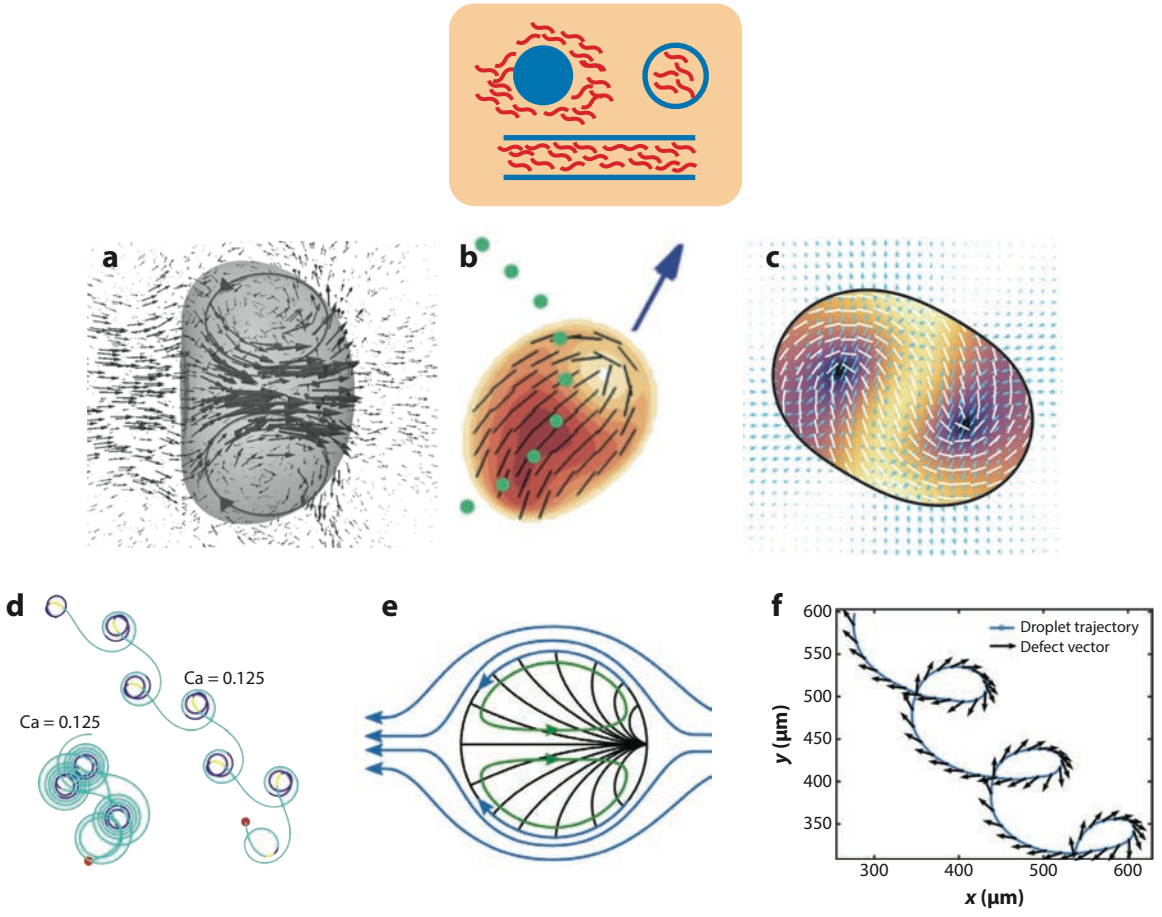

Figure 13

Type VIII systems: many swimmers near a large deformable obstacle. (*a*) A broken symmetry with nonmotile stress-generating particles under soft confinement leads to swimming. Panel adapted from Reference 265. (*b*) Zigzagging of an active nematic droplet. The arrow denotes the instantaneous swimming direction. Panel adapted with permission from Reference 266. (*c*,*d*) Periodic wobbling and a transition to swimming modes of a coarse-grained nonmotile suspension, tuned by the capillary number, Ca. Panels adapted from Reference 267 (CC BY 4.0). (*e*,*f*) Marangoni stresses on the surface of a liquid-crystal droplet couple to internal elastic modes resulting in coherent swimming, whereas additional symmetry-breaking results in chiral trajectories. Panels adapted with permission from Reference 268.

swimming, along with observed chiral trajectories (**Figure 13*f***; 268). For a broader discussion, see the review by Maass et al. (270).

3. SUMMARY AND OUTLOOK

We have described a proposed classification for swimming in complex fluids. The organization is based on the relationship of a swimming body to one or many obstacles in a fluid, broadly interpreted, be they molecular fluid constituents or enormous confining boundaries. The relative length- and timescales of the swimmers and obstacles, along with the concentration of swimmers, impacts the key physical principles at play and behaviors observed. We hope that this

classification not only organizes the vast research that has been conducted but also helps to highlight connections among research areas and those that are in need of more attention.

Within this classification, the extremes of dimensionless parameters are the easiest to understand and to model. Among the future topics that we envision are more complete explorations of the internal boundaries of the diagram, where the length scales and timescales of swimmers and obstacles are comparable, and the interactions of swimmers are on the precipice of a transition from dilute to collective behavior. Another future topic is further study of systems that do not fit within this three-dimensional classification space. For example, this classification can be viewed as the low Reynolds number region of a four-dimensional space with Reynolds number as an additional axis. This classification also assumes that the swimmers and obstacles have a single dominant length scale and timescale. Also absent in the classification is the obstacle concentration. For small Bn, this concentration will determine the flow properties of the suspending medium. For large Bn, we have focused on large single (isolated) obstacles or boundaries. Depending on the system type, the obstacle concentration may be an important axis to explore.

Nearly a century of effort combining biological, physical, and mathematical perspectives has established an incredible array of detailed knowledge about swimming in complex fluids. With our first steps to understand the simplest model systems behind us, we continue on to embrace the fantastic complexity of the biological realm.

> "It takes more than a knock on the head to kill a scientist. . . .All that mathematics makes the skull as hard as a rock, eh?"
>
> —Dr. Jan Benes, *Fantastic Voyage* by Isaac Asimov (Reference 17)

FUTURE ISSUES

1. Additional length scales and timescales provide additional axes to explore. Inertial effects would appear along another axis related to the Reynolds number. Obstacle volume fraction is another. Some systems may have multiple important swimmer length scales, like the cell body size, the flagellum diameter, and run length of a random-walk motion. Systems may have an important timescale related to their motion as individuals but also a timescale related to dynamics of the group.
2. Many studies focus on well-controlled combinations of a single type of swimmer and a single type of complex fluid, whereas many applications of interest are mixtures. Heterogeneous and multiscale systems continue to need attention.
3. Within each type, the system behavior depends on the specifics of swimmer actuation, swimming gait, and deformability. This dependence will be particularly important when seeking to understand natural biological systems and engineering new synthetic systems.
4. Systems at the boundaries between identified types are expected to combine emergent features from the extremes of the classification system. Transitions between extreme behaviors may be smooth or sudden.
5. Among the eight presented system types, Type VI systems (active suspensions in fluids with bulk complex features) are particularly challenging and understudied, both experimentally and theoretically.

6. The areas of systems and synthetic biology have expanded our understanding of internal biological processes, including how they may change in response to their environment. Coupling these internal processes with the external complex fluid behaviors described here will be an important future direction.

DISCLOSURE STATEMENT

The authors are not aware of any affiliations, memberships, funding, or financial holdings that might be perceived as affecting the objectivity of this review.

ACKNOWLEDGMENTS

We gratefully acknowledge Gwynn Elfring for helpful conversations and for critically reading the manuscript. S.E.S. acknowledges the support of the National Science Foundation (NSF)/National Institutes of Health (NIH) (DMS-1661900, DMR-2003819). P.T.U. acknowledges the support of the NSF (CBET-0954445, DMS-1211665).

LITERATURE CITED

1. Ganias K, Mezarli C, Voultsiadou E. 2017. *Fish Fisheries* 18:1038–55
2. Lighthill J. 1976. *SIAM Rev.* 18:161–230
3. Lauga E, Powers T. 2009. *Rep. Prog. Phys.* 72:096601
4. Elgeti J, Winkler RG, Gompper G. 2015. *Rep. Prog. Phys.* 78:056601
5. Lauga E. 2016. *Annu. Rev. Fluid Mech.* 48:105–30
6. Gompper G, Winkler RG, Speck T, Solon A, Nardini C, et al. 2020. *J. Phys. Condens. Matter* 32:193001
7. Spagnolie SE, ed. 2015. *Complex Fluids in Biological Systems: Experiment, Theory, and Computation*. New York: Springer
8. Purcell EM. 1977. *Am. J. Phys.* 45:3–11
9. Childress S. 1981. *Mechanics of Swimming and Flying*. Cambridge, UK: Cambridge Univ. Press
10. Larson RG. 1999. *The Structure and Rheology of Complex Fluids*, Vol. 150, Topics in Chemical Engineering, ed. KE Gubbins. New York: Oxford Univ. Press
11. Hatwalne Y, Ramaswamy S, Rao M, Simha RA. 2004. *Phys. Rev. Lett.* 92:118101
12. Ishikawa T, Pedley TJ. 2007. *J. Fluid Mech.* 588:399–435
13. Haines BM, Aranson IS, Berlyand L, Karpeev DA. 2008. *Phys. Biol.* 5:046003
14. Sokolov A, Aranson IS. 2009. *Phys. Rev. Lett.* 103:148101
15. Saintillan D. 2018. *Annu. Rev. Fluid Mech.* 50:563–92
16. Bechinger C, Di Leonardo R, Löwen H, Reichhardt C, Volpe G, Volpe G. 2016. *Rev. Mod. Phys.* 88:045006
17. Asimov I. 1966. *Fantastic Voyage*. New York: Bantam Dell
18. Reiner M. 1964. *Phys. Today* 17:62
19. Brennen C, Winet H. 1977. *Annu. Rev. Fluid Mech.* 9:339–98
20. Taylor GI. 1951. *Proc. Roy. Soc. A* 209:447–61
21. Blake JR. 1971. *J. Fluid Mech.* 46:199–208
22. Leiderman K, Olson SD. 2016. *Phys. Fluids* 28:021902
23. Ho N, Leiderman K, Olson S. 2008. *J. Fluid Mech.* 864:1088–124
24. Nganguia H, Pak OS. 2018. *J. Fluid Mech.* 855:554–73
25. Leshansky AM. 2009. *Phys. Rev. E* 80:051911
26. Jung S. 2010. *Phys. Fluids* 22:031903
27. Hewitt DR, Balmforth NJ. 2017. *J. Fluid Mech.* 828:33–56
28. Kim S, Karrila SJ. 2013. *Microhydrodynamics: Principles and Selected Applications*. New York: Dover

29. Chen Y, Lordi N, Taylor M, Pak OS. 2020. *Phys. Rev. E* 102:043111
30. Hewitt D. 2022. *Sci. Talks* 3:100029
31. Maladen RD, Ding Y, Li C, Goldman DI. 2009. *Science* 325:314–18
32. Hosoi A, Goldman D. 2015. *Annu. Rev. Fluid Mech* 47:431–53
33. Krieger MS, Spagnolie SE, Powers T. 2015. *Soft Matter* 11:9115–25
34. Cupples G, Dyson RJ, Smith DJ. 2017. *J. Fluid Mech.* 812:501–24
35. Shi J, Powers TR. 2017. *Phys. Rev. Fluids* 2:123102
36. Suarez SS, Pacey AA. 2006. *Hum. Reprod. Update* 12:23–37
37. Fauci LJ, Dillon R. 2006. *Annu. Rev. Fluid Mech.* 38:371–94
38. Morozov A, Spagnolie SE. 2015. See Reference 7, pp. 3–52
39. Vélez-Cordero JR, Lauga E. 2013. *J. Non-Newtonian Fluid Mech.* 199:37–50
40. Vasquez PA, Forest MG. 2015. See Reference 7, pp. 53–110
41. Gagnon DA, Keim NC, Arratia PE. 2014. *J. Fluid Mech.* 758:R3
42. Demir E, Lordi N, Ding Y, Pak OS. 2020. *Phys. Rev. Fluids* 5:111301
43. Li G, Ardekani AM. 2015. *J. Fluid Mech.* 784:R4
44. Park JS, Kim D, Shin JH, Weitz DA. 2016. *Soft Matter* 12:1892–97
45. Gómez S, Godínez FA, Lauga E, Zenit R. 2017. *J. Fluid Mech.* 812:R3
46. Man Y, Lauga E. 2015. *Phys. Rev. E* 92:023004
47. Datt C, Zhu L, Elfring GJ, Pak OS. 2015. *J. Fluid Mech.* 784:R1
48. Suarez SS, Dai X. 1992. *Biol. Reprod.* 46:686–91
49. Shen XN, Arratia PE. 2011. *Phys. Rev. Lett.* 106:208101
50. Ho HC, Suarez SS. 2001. *Reproduction* 122:519–26
51. Ives TR, Morozov A. 2017. *Phys. Fluids* 29:121612
52. Li L, Spagnolie SE. 2015. *Phys. Fluids* 27:021902
53. Teran J, Fauci L, Shelley M. 2010. *Phys. Rev. Lett.* 104:038101
54. Thomases B, Guy RD. 2014. *Phys. Rev. Lett.* 113:098102
55. Liu B, Powers TR, Breuer KS. 2011. *PNAS* 108:19516
56. Spagnolie SE, Liu B, Powers TR. 2013. *Phys. Rev. Lett.* 111:068101
57. Martinez VA, Schwarz-Linek J, Reufer M, Wilson LG, Morozov AN, Poon WC. 2014. *PNAS* 111:17771–76
58. Narinder N, Gomez-Solano JR, Bechinger C. 2019. *New J. Phys.* 21:093058
59. Gomez-Solano JR, Blokhuis A, Bechinger C. 2016. *Phys. Rev. Lett.* 116:138301
60. Natale G, Datt C, Hatzikiriakos SG, Elfring GJ. 2017. *Phys. Fluids* 29:123102
61. Sznitman J, Arratia P. 2015. See Reference 7, pp. 245–81
62. Elfring GJ, Lauga E. 2015. See Reference 7, pp. 283–317
63. Li G, Lauga E, Ardekani AM. 2021. *J. Non-Newtonian Fluid Mech.* 297:104655
64. Patteson AE, Gopinath A, Arratia PE. 2016. *Curr. Opin. Colloid Interface Sci.* 21:86–96
65. Lauga E. 2007. *Phys. Fluids* 19:083104
66. Balmforth NJ, Coombs D, Pachmann S. 2010. *Q. J. Mech. Appl. Math.* 63:267–94
67. Fu HC, Powers TR, Wolgemuth HC. 2007. *Phys. Rev. Lett.* 99:258101–105
68. Fu HC, Wolgemuth CW, Powers TR. 2009. *Phys. Fluids* 21:033102
69. Elfring GJ, Goyal G. 2016. *J. Non-Newtonian Fluid Mech.* 234:8–14
70. Riley EE, Lauga E. 2014. *Europhys. Lett.* 108:34003
71. Riley EE, Lauga E. 2015. *J. Theor. Biol.* 382:345–55
72. Pak OS, Normand T, Lauga E. 2010. *Phys. Rev. E* 81:036312
73. Li GJ, Karimi A, Ardekani AM. 2014. *Rheol. Acta* 53:911–26
74. Binagia JP, Phoa A, Housiadas KD, Shaqfeh ESG. 2020. *J. Fluid Mech.* 900:A4
75. Binagia JP, Shaqfeh ESG. 2021. *Phys. Rev. Fluids* 6(5):053301
76. Berg HC, Turner L. 1979. *Nature* 278:349–51
77. Kimsey RB, A. S. 1990. *J. Infect. Dis.* 162:1205–8
78. Zhang Y, Li G, Ardekani AM. 2018. *Phys. Rev. Fluids* 3(2):023101
79. Pak OS, Zhu L, Brandt L, Lauga E. 2012. *Phys. Fluids* 24(10):103102

80. Wu Z, Chen Y, Mukasa D, Pak OS, Gao W. 2020. *Chem. Soc. Rev.* 49(22):8088–112
81. Kroo LA, Binagia JP, Eckman N, Prakash M, Shaqfeh ESG. 2022. *J. Fluid Mech.* 944:A20
82. Venugopalan PL, Esteban-Fernández de Ávila B, Pal M, Ghosh A, Wang J. 2020. *ACS Nano* 14(8):9423–39
83. Petrou G, Crouzier T. 2018. *Biomater. Sci.* 6(9):2282–97
84. Fu HC, Shenoy VB, Powers TR. 2010. *Europhys. Lett.* 91:24002
85. Du J, Keener JP, Guy RD, Fogelson AL. 2012. *Phys. Rev. E* 85:036304
86. Schamel D, Mark AG, Gibbs JG, Miksch C, Morozov KI, et al. 2014. *ACS Nano* 8:8794–801
87. Celli JP, Turner BS, Afdhal NH, Keates S, Ghiran I, et al. 2009. *PNAS* 106:14321–26
88. Chrétien FC. 2003. *Acta Obstet. Gynecol. Scand.* 82:449–61
89. Wróbel JK, Lynch S, Barrett A, Fauci L, Cortez R. 2016. *J. Fluid Mech.* 792:775–97
90. Viney C, Huber AE, Verdugo P. 1993. *Macromolecules* 26:852–55
91. Zhou S, Sokolov A, Lavrentovich OD, Aranson IS. 2014. *PNAS* 111:1265–70
92. Mushenheim PC, Trivedi RR, Weibel DB, Abbott NL. 2014. *Biophys. J.* 107:255–65
93. Trivedi RR, Maeda R, Abbott NL, Spagnolie SE, Weibel DB. 2015. *Soft Matter* 11:8404–8
94. Genkin MM, Sokolov A, Lavrentovich OD, Aranson IS. 2017. *Phys. Rev. X* 7:011029
95. Krieger MS, Spagnolie SE, Powers TR. 2019. *J. Non-Newtonian Fluid Mech.* 273:104185
96. Lin Z, Chen S, Gao T. 2021. *J. Fluid Mech.* 921:A25
97. Nayani K, Córdova-Figueroa UM, Abbott NL. 2019. *Langmuir* 36:6948–56
98. De Gennes PG, Prost J. 1993. *The Physics of Liquid Crystals*. Oxford, UK: Oxford Univ. Press
99. Peng C, Turiv T, Guo Y, Wei QH, Lavrentovich OD. 2016. *Science* 354:882–85
100. Katz DF. 1974. *J. Fluid Mech.* 64:33–49
101. Rothschild LJ. 1963. *Nature* 198:1221–22
102. Smith DJ, Blake JR. 2009. *Math. Sci.* 34:74–87
103. Bianchi S, Saglimbeni F, Di Leonardo R. 2017. *Phys. Rev. X* 7:011010
104. Kantsler V, Dunkel J, Polin M, Goldstein RE. 2013. *PNAS* 110:1187–92
105. Brosseau Q, Usabiaga FB, Lushi E, Wu Y, Ristroph L, et al. 2021. *Soft Matter* 17:6597–602
106. Spagnolie SE, Lauga E. 2012. *J. Fluid. Mech.* 700:1–43
107. Smith DJ, Gaffney EA, Blake JR, Kirkman-Brown JC. 2009. *J. Fluid Mech.* 621:289–320
108. Mousavi SM, Gompper G, Winkler RG. 2020. *Soft Matter* 16:4866–75
109. Mathijssen AJ, Figueroa-Morales N, Junot G, Clément E, Lindner A, Zöttl A. 2019. *Nat. Commun.* 10:1–12
110. Chen H, Thiffeault JL. 2021. *J. Fluid Mech.* 916:A15
111. Zhu L, Lauga E, Brandt L. 2013. *J. Fluid Mech.* 726:285–311
112. Jana S, Um SH, Jung S. 2012. *Phys. Fluids* 24:041901
113. Chrispell JC, Fauci LJ, Shelley M. 2013. *Phys. Fluids* 25:e1002167
114. Berg HC, Turner L. 1990. *Biophys. J.* 58:919–930
115. Frymier PD, Ford RM, Berg HC, Cummings PT. 1995. *PNAS* 92:6195–99
116. Lauga E, DiLuzio WR, Whitesides GM, Stone HA. 2006. *Biophys. J.* 90:400–12
117. Lushi E, Kantsler V, Goldstein RE. 2017. *Phys. Rev. E* 96:023102
118. Turner L, Ryu WS, Berg HC. 2000. *J. Bacteriol.* 182:2793–801
119. Molaei M, Barry M, Stocker R, Sheng J. 2014. *Phys. Rev. Lett.* 113:068103
120. Buchner AJ, Muller K, Mehmood J, Tam D. 2021. *PNAS* 118(20):e2102095118
121. Llopis I, Pagonabarraga I. 2010. *J. Non-Newtonian Fluid Mech.* 165:946–52
122. Goto T, Nakata K, Baba K, Nishimura M, Magariyama Y. 2005. *Biophys. J.* 89:3771–79
123. Giacché D, Ishikawa T, Yamaguchi T. 2010. *Phys. Rev. E* 82:056309
124. Shum H, Gaffney EA, Smith DJ. 2010. *Proc. Roy. Soc. A* 466:1725–48
125. Elgeti J, Kaupp UB, Gompper G. 2010. *Biophys. J.* 99:1018–26
126. Hill J, Kalkanci O, McMurry JL, Koser H. 2007. *Phys. Rev. Lett.* 98:068101
127. Ishimoto K, Crowdy DG. 2017. *J. Fluid Mech.* 821:647–67
128. Figueroa-Morales N, Mino GL, Rivera A, Caballero R, Clément E, et al. 2015. *Soft Matter* 11(31):6284–93

129. Li G, Tang JX. 2009. *Phys. Rev. Lett.* 103:078101
130. Schaar K, Zöttl A, Stark H. 2015. *Phys. Rev. Lett.* 115:038101
131. Tokárová V, Perumal AS, Nayak M, Shum H, Kašpar O, et al. 2021. *PNAS* 118(17):e2013925118
132. Crowdy DG, Or Y. 2010. *Phys. Rev. E* 81:036313
133. Or Y, Zhang S, Murray RM. 2011. *SIAM J. Appl. Dyn. Sys.* 10:1013–41
134. Zöttl A, Stark H. 2012. *Phys. Rev. Lett.* 108:218104
135. Spagnolie SE, Wahl C, Lukasik J, Thiffeault JL. 2017. *Physica D* 341:33–44
136. Liu B, Breuer KS, Powers TR. 2014. *Phys. Fluids* 26:011701
137. LaGrone J, Cortez R, Fauci L. 2019. *Phys. Rev. Fluids* 4:033102
138. Lebois F, Sauvage P, Py C, Cardoso O, Ladoux B, et al. 2012. *Biophys. J.* 102:2791–98
139. Takagi D, Palacci J, Braunschweig AB, Shelley MJ, Zhang J. 2014. *Soft Matter* 10:1784–89
140. Sipos O, Nagy K, Di Leonardo R, Galajda P. 2015. *Phys. Rev. Lett.* 114:258104
141. Spagnolie SE, Moreno-Flores GR, Bartolo D, Lauga E. 2015. *Soft Matter* 11:3396–411
142. Makarchuk S, Braz VC, Araújo NA, Ciric L, Volpe G. 2019. *Nat. Commun.* 10:1–12
143. Wykes MSD, Zhong X, Tong J, Adachi T, Liu Y, et al. 2017. *Soft Matter* 13:4681–88
144. Mathijssen AJTM, Jeanneret R, Polin M. 2018. *Phys. Rev. Fluids* 3:033103
145. Alonso-Matilla R, Chakrabarti B, Saintillan D. 2019. *Phys. Rev. Fluids* 4:043101
146. Brown AT, Vladescu ID, Dawson A, Vissers T, Schwarz-Linek J, et al. 2016. *Soft Matter* 12:131–40
147. Bhattacharjee T, Datta SS. 2019. *Nat. Commun.* 10:1–9
148. Park S, Hwang H, Nam SW, Martinez F, Austin RH, Ryu WS. 2008. *PLOS ONE* 3:e2550
149. Wysocki A, Elgeti J, Gompper G. 2015. *Phys. Rev. E* 91:050302
150. Contino M, Lushi E, Tuval I, Kantsler V, Polin M. 2015. *Phys. Rev. Lett.* 115:258102
151. Mozaffari A, Sharifi-Mood N, Koplik J, Maldarelli C. 2016. *Phys. Fluids* 28:053107
152. Lintuvuori JS, Brown AT, Stratford K, Marenduzzo D. 2016. *Soft Matter* 12:7959–68
153. Galajda P, Keymer J, Chaikin P, Austin R. 2007. *J. Bacteriol.* 189:8704–7
154. Mueller P, Thiffeault JL. 2017. *Phys. Rev. Fluids* 2:013103
155. Lin Z, Thiffeault JL, Childress S. 2011. *J. Fluid Mech.* 669:167–77
156. Shum H, Yeomans JM. 2017. *Phys. Rev. Fluids* 2:113101
157. Kamdar S, Shin S, Leishangthem P, Francis LF, Xu X, Cheng X. 2022. *Nature* 603(7903):819–23
158. Majmudar T, Keaveny EE, Zhang J, Shelley MJ. 2012. *J. Roy. Soc. Interface* 9(73):1809–23
159. Conrad JC. 2020. *J. Ind. Microbiol. Biotechnol.* 47:725–38
160. Mathijssen AJ, Doostmohammadi A, Yeomans JM, Shendruk TN. 2016. *J. Fluid Mech.* 806:35–70
161. Morse M, Huang A, Li G, Maxey MR, Tang JX. 2013. *Biophys. J.* 105:21–28
162. Lopez D, Lauga E. 2014. *Phys. Fluids* 26:400–12
163. Deng J, Molaei M, Chisholm NG, Stebe KJ. 2020. *Langmuir* 36:6888–902
164. Sprenger AR, Shaik VA, Ardekani AM, Lisicki M, Mathijssen AJTM, et al. 2020. *Euro. Phys. J. E* 43:1–18
165. Crowdy D, Lee S, Samson O, Lauga E, Hosoi AE. 2011. *J. Fluid Mech.* 681:24–47
166. Dias MA, Powers TR. 2013. *Phys. Fluids* 25:101901
167. Ledesma-Aguilar R, Yeomans JM. 2013. *Phys. Rev. Lett.* 111:138101
168. Lemelle L, Palierne JF, Chatre E, Place C. 2010. *J. Bacteriol.* 192:6307–8
169. Bianchi S, Saglimbeni F, Frangipane G, Dell'Arciprete D, Di Leonardo R. 2019. *Soft Matter* 15:3397–406
170. Di Leonardo R, Dell'Arciprete D, Angelani L, Iebba V. 2011. *Phys. Rev. Lett.* 106:038101
171. Pimponi D, Chinappi M, Gualtieri P, Casciola CM. 2016. *J. Fluid Mech.* 789:514–33
172. Desai N, Shaik VA, Ardekani AM. 2018. *Soft Matter* 14:264–78
173. Shaik VA, Ardekani AM. 2019. *Phys. Rev. E* 99:033101
174. Ahmadzadegan A, Wang S, Vlachos PP, Ardekani AM. 2019. *Phys. Rev. E* 100:062605
175. Trouilloud R, Yu T, Hosoi A, Lauga E. 2008. *Phys. Rev. Lett.* 101:048102
176. Shaik VA, Ardekani AM. 2017. *J. Fluid Mech.* 824:42–73
177. Wu H, Thiébaud M, Hu WF, Farutin A, Rafai S, et al. 2015. *Phys. Rev. E* 92:050701
178. Dalal S, Farutin A, Misbah C. 2020. *Soft Matter* 16:1599–613
179. Woolley DM, Crockett RF, Groom WD, Revell SG. 2009. *J. Exp. Biol.* 212:2215–23
180. Yuan J, Raizen DM, Bau H. 2014. *PNAS* 111:6865–70

181. Dombrowski C, Cisneros L, Chatkaew S, Goldstein RE, Kessler JO. 2004. *Phys. Rev. Lett.* 93:098103
182. Hernandez-Ortiz JP, Stoltz CG, Graham MD. 2005. *Phys. Rev. Lett.* 95:204501
183. Saintillan D, Shelley MJ. 2007. *Phys. Rev. Lett.* 99:058102
184. Evans AA, Ishikawa T, Yamaguchi T, Lauga E. 2011. *Phys. Fluids* 23:111702
185. Schoeller SF, Keaveny EE. 2018. *J. Roy. Soc. Interface* 15:20170834
186. Saintillan D, Shelley MJ. 2013. *C. R. Phys.* 14:497–517
187. Miles CJ, Evans AA, Shelley MJ, Spagnolie SE. 2019. *Phys. Rev. Lett.* 122:098002
188. Ramaswamy S. 2010. *Annu. Rev. Condens. Matter Phys.* 1:323–45
189. Koch DL, Subramanian G. 2011. *Annu. Rev. Fluid Mech.* 43:637–59
190. Vicsek T, Zafeiris A. 2012. *Phys. Rep.* 517:71–140
191. Marchetti MC, Joanny JF, Ramaswamy S, Liverpool TB, Prost J, et al. 2013. *Rev. Mod. Phys.* 85:1143
192. Saintillan D, Shelley MJ. 2015. See Reference 7, pp. 319–55
193. Alert R, Casademunt J, Joanny JF. 2022. *Annu. Rev. Condens. Matter Phys.* 13:143–70
194. Gachelin J, Rousselet A, Lindner A, Clement E. 2014. *New J. Phys.* 16:025003
195. Patteson A, Gopinath A, Purohit PK, Arratia PE. 2016. *Soft Matter* 12(8):2365–72
196. Peng Y, Lai L, Tai YS, Zhang K, Xu X, Cheng X. 2016. *Phys. Rev. Lett.* 116(6):068303
197. Soni V, Bililign ES, Magkiriadou S, Sacanna S, Bartolo D, et al. 2019. *Nat. Phys.* 15(11):1188–94
198. Han K, Kokot G, Tovkach O, Glatz A, Aranson IS, Snezhko A. 2020. *PNAS* 117(18):9706–11
199. Shankar S, Souslov A, Bowick MJ, Marchetti MC, Vitelli V. 2022. *Nat. Rev. Phys.* 4(6):380–98
200. Petroff AP, Wu X-L, Libchaber A. 2015. *Phys. Rev. Lett.* 114(15):158102
201. Tan TH, Mietke A, Li J, Chen Y, Higinbotham H, et al. 2022. *Nature* 607:287–93
202. Underhill PT, Hernandez-Ortiz JP, Graham MD. 2008. *Phys. Rev. Lett.* 100:248101
203. Ishikawa T, Locsei J, Pedley T. 2008. *J. Fluid Mech.* 615:401–31
204. Underhill PT, Graham MD. 2011. *Phys. Fluids* 23:121902
205. Saintillan D, Shelley MJ. 2012. *J. Roy. Soc. Interface* 9:571–85
206. Bárdfalvy D, Nordanger H, Nardini C, Morozov A, Stenhammar J. 2019. *Soft Matter* 15:7747–56
207. Kasyap T, Koch DL, Wu M. 2014. *Phys. Fluids* 26(8):081901
208. Morozov A, Marenduzzo D. 2014. *Soft Matter* 10(16):2748–58
209. Stenhammar J, Nardini C, Nash RW, Marenduzzo D, Morozov A. 2017. *Phys. Rev. Lett.* 119:028005
210. Brotto T, Bartolo D, Saintillan D. 2015. *J. Nonlinear Sci.* 25:1125–39
211. Schoeller SF, Holt WV, Keaveny EE. 2020. *Philos. Trans. Roy. Soc. B* 375:20190384
212. Simha RA, Ramaswamy S. 2002. *Phys. Rev. Lett.* 89:058101
213. Qian Y, Kramer PR, Underhill PT. 2017. *Phys. Rev. Fluids* 2:043104
214. Škultéty V, Nardini C, Stenhammar J, Marenduzzo D, Morozov A. 2020. *Phys. Rev. X* 10:031059
215. Rafaï S, Jibuti L, Peyla P. 2010. *Phys. Rev. Lett.* 104:098102
216. Mussler M, Rafaï S, Peyla P, Wagner C. 2013. *Europhys. Lett.* 101:54004
217. Gachelin J, Mino G, Berthet H, Lindner A, Rousselet A, Clément É. 2013. *Phys. Rev. Lett.* 110:268103
218. López HM, Gachelin J, Douarche C, Auradou H, Clément E. 2015. *Phys. Rev. Lett.* 115:028301
219. McDonnell AG, Gopesh TC, Lo J, O'Bryan M, Yeo LY, et al. 2015. *Soft Matter* 11:4658–68
220. Saintillan D. 2010. *Phys. Rev. E* 81(5):056307
221. Guo S, Samanta D, Peng Y, Xu X, Cheng X. 2018. *PNAS* 115(28):7212–17
222. Takatori S, Brady J. 2017. *Phys. Rev. Lett.* 118:018003
223. Ishikawa T, Brumley DR, Pedley TJ. 2021. *J. Fluid Mech.* 914:A26
224. Matsui H, Omori T, Ishikawa T. 2020. *Phys. Fluids* 32:071902
225. Bozorgi Y, Underhill PT. 2014. *Rheol. Acta* 53(12):899–909
226. Bechtel TM, Khair AS. 2017. *Rheol. Acta* 56:149–60
227. Cates M, Fielding S, Marenduzzo D, Orlandini E, Yeomans J. 2008. *Phys. Rev. Lett.* 101:068102
228. Giomi L, Liverpool TB, Marchetti MC. 2010. *Phys. Rev. E* 81:051908
229. Liu Z, Zhang K, Cheng X. 2019. *Rheol. Acta* 58(8):439–51
230. Hochbaum AI, Aizenberg J. 2010. *Nano Lett.* 10:3717–21
231. Elfring GJ, Pak OS, Lauga E. 2010. *J. Fluid Mech.* 646:505–15
232. Tung CK, Lin C, Harvey B, Fiore AG, Ardon F, et al. 2017. *Sci. Rep.* 7:1–9

233. Sokolov A, Zhou S, Lavrentovich OD, Aranson IS. 2015. *Phys. Rev. E* 91:013009
234. Zhou S, Tovkach O, Golovaty D, Sokolov A, Aranson IS, Lavrentovich OD. 2017. *New J. Phys.* 19:055006
235. Liu S, Shankar S, Marchetti MC, Wu Y. 2021. *Nature* 590:80–84
236. Bozorgi Y, Underhill PT. 2014. *J. Non-Newtonian Fluid Mech.* 214:69–77
237. Li G, Ardekani AM. 2016. *Phys. Rev. Lett.* 117:118001
238. Bozorgi Y, Underhill PT. 2011. *Phys. Rev. E* 84:061901
239. Bozorgi Y, Underhill PT. 2013. *J. Rheol.* 57:511
240. Caldara M, Friedlander RS, Kavanaugh NL, Aizenberg J, Foster KR, Ribbeck K. 2012. *Curr. Biol.* 22:2325–30
241. Wagner CE, Wheeler KM, Ribbeck K. 2018. *Annu. Rev. Cell Dev. Biol.* 34:189–215
242. Lushi E, Wioland H, Goldstein RE. 2014. *PNAS* 111:9733–38
243. Wioland H, Woodhouse FG, Dunkel J, Goldstein RE. 2016. *Nat. Phys.* 12:341–45
244. Wioland H, Lushi E, Goldstein RE. 2016. *New J. Phys.* 18:075002
245. Theillard M, Saintillan D. 2019. *J. Comput. Phys.* 397:108841
246. Riedel IH, Kruse K, Howard J. 2005. *Science* 309:300–3
247. Angelani L, Maggi C, Bernardini ML, Rizzo A, Di Leonardo R. 2011. *Phys. Rev. Lett.* 107:138302
248. Singh J, Patteson AE, Maldonado BOT, Purohit PK, Arratia PE. 2021. *Soft Matter* 17:4151–60
249. Reinken H, Nishiguchi D, Heidenreich S, Sokolov A, Bär M, et al. 2020. *Commun. Phys.* 3:1–9
250. Theillard M, Alonso-Matilla R, Saintillan D. 2017. *Soft Matter* 13:363–75
251. Zöttl A, Stark H. 2014. *Phys. Rev. Lett.* 112:118101
252. Hernandez-Ortiz JP, Underhill PT, Graham MD. 2009. *J. Phys. Cond. Matt.* 21:204107
253. Driscoll M, Delmotte B, Youssef M, Sacanna S, Donev A, Chaikin P. 2017. *Nat. Phys.* 13:375–79
254. van Zuiden BC, Paulose J, Irvine WTM, Bartolo D, Vitelli V. 2016. *PNAS* 113(46):12919–24
255. Dasbiswas K, Mandadapu KK, Vaikuntanathan S. 2018. *PNAS* 115(39):E9031–40
256. Yang X, Ren C, Cheng K, Zhang HP. 2020. *Phys. Rev. E* 101(2):022603
257. Liu P, Zhu H, Zeng Y, Du G, Ning L, et al. 2020. *PNAS* 117(22):11901–7
258. Zhang B, Hilton B, Short C, Souslov A, Snezhko A. 2020. *Phys. Rev. Res.* 2(4):043225
259. Vaccari L, Molaei M, Niepa TH, Lee D, Leheny RL, Stebe KJ. 2017. *Adv. Colloid Interface Sci.* 247:561–72
260. Dorobantu LS, Yeung AK, Foght JM, Gray MR. 2004. *Appl. Env. Microbiol.* 70:6333–36
261. Rivas DP, Hedgecock ND, Stebe KJ, Leheny RL. 2021. *Soft Matter* 17:8195–210
262. Mazza MG. 2016. *J. Phys. D Appl. Phys.* 49(20):203001
263. Costerton JW, Stewart PS, Greenberg EP. 1999. *Science* 284:1318–22
264. Sanchez T, Chen DTN, DeCamp SJ, Heymann M, Dogic Z. 2012. *Nature* 491:431–34
265. Tjhung E, Marenduzzo D, Cates ME. 2012. *PNAS* 109:12381–86
266. Gao T, Li Z. 2017. *Phys. Rev. Lett.* 119:108002
267. Young YN, Shelley MJ, Stein DB. 2021. *Math. Biosci. Eng.* 18:2849–81
268. Krüger C, Klös G, Bahr C, Maass CC. 2016. *Phys. Rev. Lett.* 117:048003
269. Whitfield CA, Hawkins RJ. 2016. *New J. Phys.* 18:123016
270. Maass CC, Krüger C, Herminghaus S, Bahr C. 2016. *Annu. Rev. Condens. Matter Phys.* 7:171–93

Annual Review of Condensed Matter Physics

Volume 14, 2023

Contents

Errata

An online log of corrections to *Annual Review of Condensed Matter Physics* articles may be found at http://www.annualreviews.org/errata/conmatphys